### DOI: 10.1002/pro.70033

### RESEARCH ARTICLE



# Citrullination at the N-terminal region of MDM2 by the PADI4 enzyme

José L. Neira<sup>1,2</sup> | Bruno Rizzuti<sup>2,3</sup> | Martina Palomino-Schätzlein<sup>4</sup> Virginia Rejas<sup>5</sup> | Olga Abian<sup>2,6,7,8</sup> | Adrian Velazquez-Campoy<sup>2,6,7,8</sup> |

<sup>1</sup>IDIBE, Universidad Miguel Hernández, Elche, Alicante, Spain

<sup>2</sup>Instituto de Biocomputación y Física de Sistemas Complejos (BIFI), Universidad de Zaragoza, Zaragoza, Spain

<sup>3</sup>CNR-NANOTEC, SS Rende (CS), Department of Physics, University of Calabria, Rende, Italy

<sup>4</sup>ProtoQSAR SL, CEEI-Valencia. Parque Tecnológico de Valencia, Paterna, Valencia, Spain

<sup>5</sup>Centro de Investigación Príncipe Felipe, Calle de Eduardo Primo Yufera 3, Valencia, Spain

<sup>6</sup>Instituto de Investigación Sanitaria Aragón (IIS Aragón), Zaragoza, Spain

<sup>7</sup>Centro de Investigación Biomédica en Red en el Área Temática de Enfermedades Hepáticas y Digestivas (CIBERehd), Madrid, Spain

<sup>8</sup>Departamento de Bioquímica y Biología Molecular y Celular, Universidad de Zaragoza, Zaragoza, Spain

### Correspondence

José L. Neira, IDIBE, Edificio Torregaitán, Universidad Miguel Hernández, Avda. del Ferrocarril s/n, 03202 Elche, Alicante, Spain.

Email: jlneira@umh.es

#### Funding information

European Commission; Diputacion General de Aragon; Ministerio de Ciencia e Innovación; Instituto de Salud Carlos III; Generalitat Valenciana

Review Editor: Jeanine Amacher

#### **Abstract**

PADI4 is one of the human isoforms of a family of enzymes involved in the conversion of arginine to citrulline. MDM2 is an E3 ubiquitin ligase that is critical for degradation of the tumor suppressor gene p53. We have previously shown that there is an interaction between MDM2 and PADI4 in cellulo, and that such interaction occurs through the N-terminal region of MDM2, N-MDM2, and in particular through residues Thr26, Val28, Phe91, and Lys98. Here, by using a "divide-and-conquer" approach, we have designed and synthesized peptides comprising these two polypeptide stretches (residues Ala21-Lys36, and Lys94-Val108), either in the wild-type species or in their citrullinated versions. Some of the citrullinated peptides were aggregation-prone, as suggested by DOSY-NMR experiments, but the wild-type versions of both fragments were monomeric in solution. We found out that wild-type and modified peptides were disordered in all cases, as also tested by far-UV circular dichroism (CD), and citrullination mainly affected the NMR chemical shifts of adjacent residues. Isothermal titration calorimetry (ITC) in the absence and presence of GSK484, an enzymatic PADI4 inhibitor, indicated that this compound blocked binding of the peptides to the enzyme. Binding to the active site of the N-MDM2 fragments was also confirmed by in silico experiments. The affinities of PADI4 for the wild-type peptides were more favorable than those of the corresponding citrullinated ones, but all measured values were within the micromolar range, indicating that there were no major variations in the thermodynamics of binding due to sequence effects. The kinetic dissociation rates,  $k_{\text{off}}$ , measured by biolayer interferometry (BLI), were always one-order of magnitude faster for the citrullinated peptides than for the wild-type ones. Taken together, all these findings indicate that MDM2 is a substrate for PADI4 and is prone to citrullination in the identified (and specific) positions of its N-terminal region.

#### KEYWORDS

isothermal titration calorimetry, MDM2, molecular docking, NMR, PADI4, peptides, protein–protein interactions

This is an open access article under the terms of the Creative Commons Attribution License, which permits use, distribution and reproduction in any medium, provided the original work is properly cited.

© 2025 The Author(s). Protein Science published by Wiley Periodicals LLC on behalf of The Protein Society.



### 1 | INTRODUCTION

PADI4 is a member of a family of peptidyl-arginine deiminases (PADI, EC 3.5.3.15), hydrolytic enzymes capable of catalyzing citrullination, that is, the conversion of arginine to citrulline residues, in the presence of Ca(II), through side chain deimination. This post-translational modification (PTM) is permanent; further, because it results in removal of an imine group and lack of proton ionization capability of the side chain, it alters the molecular properties of the polypeptide chain and it has important roles in human diseases (Gudmann et al., 2015; György et al., 2006; Ishigami & Maruyama, 2010; Yuzhalin, 2019). PADI4 is usually located in cytoplasmic granules of inflammatory cells (eosinophils, neutrophils, and macrophages), mammary gland cells, stem cells, and in tumor cells, where is highly expressed, either in the cytosol or in the nucleus. PADI4 is involved in gene transcription and immune system modulation (Wang et al., 2021; Witalison et al., 2015; Yang et al., 2021; Ying et al., 2009). Furthermore, PADI4 intervenes in p53 gene expression, as well as in the expression of other p53target genes (Li et al., 2008; Li et al., 2010; Yang et al., 2021). We have recently shown that PADI4 is expressed in glioblastoma, pancreatic adenocarcinoma, and colon cancer (Neira Araujo-Abad, et al., 2022), and it binds to other crucial proteins involved in cancer develsuch as NUPR1 (Araujo-Abad, et al., 2023), importin  $\alpha$  (Neira, et al., 2022), RING1B (Araujo-Abad et al., 2024), RYBP (Araujo-Abad, Fuentes-Baile, et al., 2023), and plakophilin 1 (Momand et al., 2000). However, it is not yet confirmed whether those proteins are substrates for PADI4 in cellulo.

The MDM2 (murine double minute 2) oncoprotein (EC. 2.3.2.27) (Momand et al., 1992; Momand et al., 2000) is a 491-residue-long E3 ubiquitin ligase encoded by the mdm2 oncogene, capable of inhibiting the protein p53 in several ways (Chen et al., 1993; Kussie et al., 1996; Momand et al., 1992). Its N-terminal region, N-MDM2, involving residues 1–125, including the well-ordered ones 27–109 (McCoy et al., 2003), is composed of four  $\alpha$ -helices (residues 32-41, 50-63, 81-86, and 96-104), a threestranded anti-parallel β-sheet (residues 66–68, 74–76, and 90–92), and another two-stranded anti-parallel one (residues 27-30 and 106-109) (Kussie et al., 1996; Uhrinova et al., 2005). We have shown that PADI4 and MDM2 interact (Araujo-Abad, Rizzuti, et al., 2023) through the N-MDM2 region, mainly by means of its residues Thr26, Val28, Phe91, and Lys98, but experiments so far did not clarify yet whether the arginines nearby these hot-spot residues, namely Arg29, Arg97, and Arg105, could be targets for PADI4.

In this work, we have used a "divide-and-conquer" approach to determine whether N-MDM2 could be a substrate of PADI4. We have synthesized two series of peptides comprising the unmodified (non-citrullinated) namely residues. Arg29, Arg97, and Arg105: (i) A<sup>21</sup>SEQETLV**R**PKPLLLK<sup>36</sup>—this sequence of the first series was modified by introducing a tyrosine at its N-terminus to allow us for determining peptide concentration by using absorbance (as described in Section 4.3); and (ii) K94EHRKIYTMIYRNLV108, and their citrullinated species in correspondence with the arginines indicated in bold: the single PTM for the first peptide (Cit29); and the two single PTMs (Cit97R105 and R97Cit105) and the double one for the second peptide (Cit97Cit105). It is important to note that we did not include other residues close to those arginines, which were reported to change the chemical shifts of their cross-peaks in previous studies, because of the use of 15N-labeled N-MDM2 (Araujo-Abad, Rizzuti, et al., 2023), to improve the solubility of the corresponding peptides. We have studied the conformational preferences of the two series of peptides by using fluorescence, far-ultraviolet (UV) circular dichroism (CD) and <sup>1</sup>H-NMR. The results show that the peptides were disordered in isolation and monomeric, except the peptide with double PTM comprising the Lys94-Val108 region and the one with the single citrullinated variant Arg105. Binding to PADI4 was monitored by fluorescence, biolayer interferometry (BLI) and isothermal titration calorimetry (ITC). The last technique was also employed for assessing the binding of the peptides in the presence and absence of GSK484, an inhibitor of PADI4 targeting its catalytic site. Binding of the peptides was abolished by the presence of the inhibitor for the two series of peptides. The affinities of PADI4 for unmodified peptides, as determined by ITC, were higher than those of the corresponding citrullinated ones, but they were all within the micromolar range, indicating that there were no major variations in the thermodynamics of binding of the peptides due to sequence effects. Finally, molecular simulations identified some structural details of the "fuzzy" binding modes of the peptides, as well as the hot-spot region of PADI4 involved in the binding. Thus, we can conclude that Arg29, Arg97, and Arg105 of N-MDM2 are target residues of PADI4. The fact that MDM2 might undergo a PTM at those positions opens the possibility to develop new cancer therapies based on its citrullination or, alternatively, to use it in liquid biopsy for early detection and prognosis of citrullinated species, or for the detection of the antigens to identify their presence.

469896x, 2025, 2, Downloaded from https

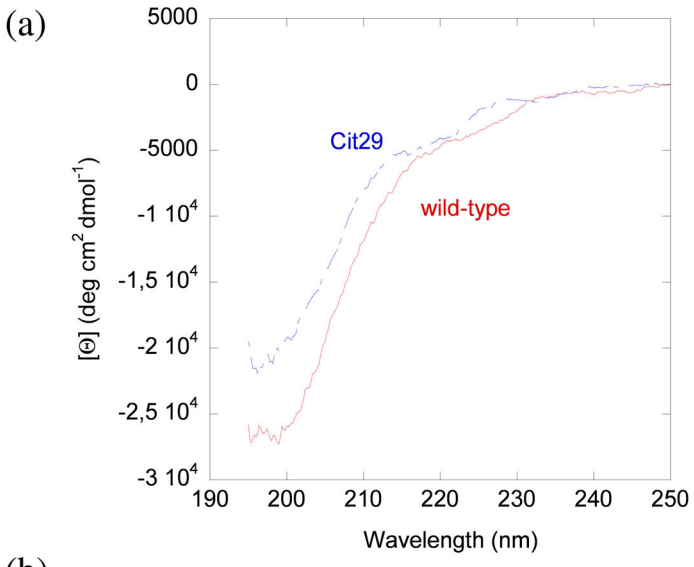
elibrary.wiley.com/doi/10.1002/pro.70033 by Universidad Miguel Hernández De Elche, Wiley Online Library on [29/10/2025]. See the

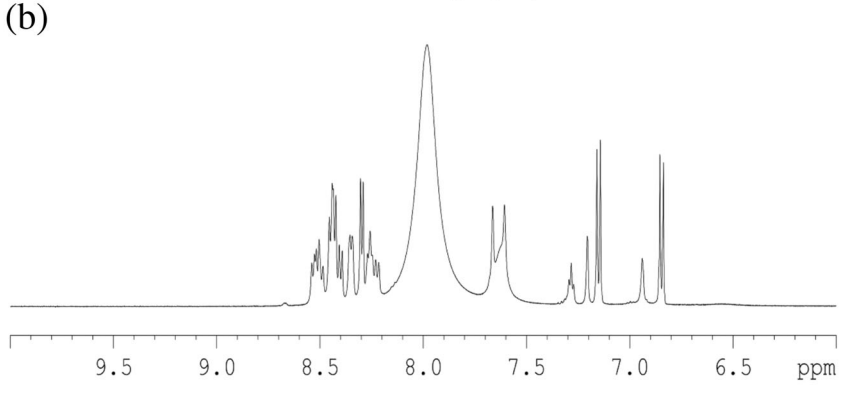
## 2 | RESULTS

# 2.1 | Conformational features and binding to PADI4 of the Ala21-Lys36 peptide series

# 2.1.1 | Conformational features of isolated Ala21–Lys36 peptides

We started to investigate the conformational properties of the Ala21–Lys36 peptides by acquiring fluorescence spectra (from a single tyrosine added at their N-terminus, as the sole residue not part of that MDM2 sequence in that region) and the far-UV CD spectra of the isolated peptides (Figure 1a). The fluorescence spectra of the two Ala21–Lys36 peptides showed a maximum at  $\sim$ 308 nm, characteristic in fact of the tyrosine residue. The far-UV CD spectra had an intense minimum at  $\sim$ 200 nm, indicating that both peptides had mostly a random-coil conformation. All spectra showed a small shoulder at 222 nm, which could be attributed to the presence of the sole reporting tyrosine (Chakrabartty et al., 1993; Kelly et al., 2005). The disordered character of the Ala21–Lys36 series was further confirmed by their 1D- $^1$ H-NMR





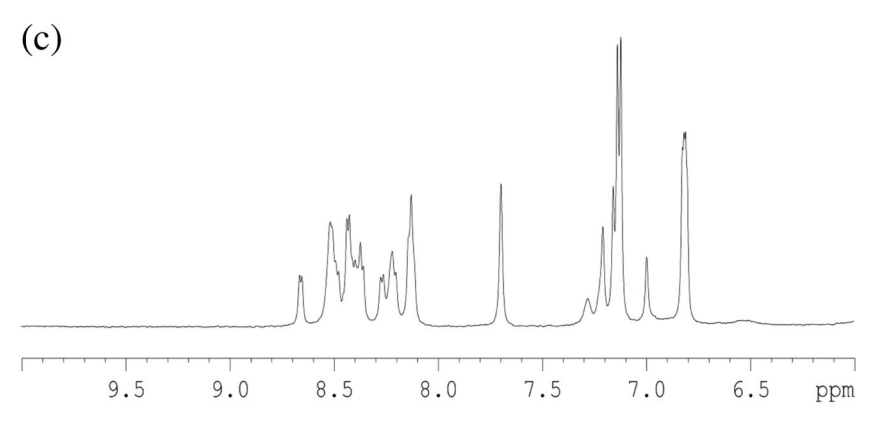


FIGURE 1 Conformational features of the isolated Ala21–Lys36 and Lys94–Val108 peptides: (a) far-UV CD of Ala21-Lys36 peptides. All spectra were normalized to the same concentration. The amide region of the 1D-¹H NMR spectra is shown for (b) the wild-type peptide Ala21–Lys36; and (c) the wild-type peptide Lys94–Val108.

1469896s, 2025, 2, Downloaded from https://onlinelibrary.wiley.com/doi/10.1002/pro.70033 by Universidad Miguel Hernández De Elche, Wiley Online Library on [29/10/2025]. See the Terms and Conditions (https://onlinelibrary.wiley.com/doi/10.1002/pro.70033 by Universidad Miguel Hernández De Elche, Wiley Online Library on [29/10/2025]. See the Terms and Conditions (https://onlinelibrary.wiley.com/doi/10.1002/pro.70033 by Universidad Miguel Hernández De Elche, Wiley Online Library on [29/10/2025]. See the Terms and Conditions (https://onlinelibrary.wiley.com/doi/10.1002/pro.70033 by Universidad Miguel Hernández De Elche, Wiley Online Library on [29/10/2025].

on Wiley Online Library for rules of use; OA articles are governed by the applicable Creative Commons

spectrum of the wild-type peptide (Figure 1b), which is similar to that of the citrullinated species. This spectrum showed a clustering of the signals of all the amide protons between 8.0 and 8.6 ppm, whereas those of the methyl protons were observed between 0.8 and 1.0 ppm (Figure S1a). All these values are characteristic of disordered chains (Cavanagh et al., 1995).

The translational diffusion coefficients, D, measured by diffusion ordered spectroscopy (DOSY) experiment were  $(2.09 \pm 0.09) \times 10^{-6} \text{ cm}^2 \text{ s}^{-1}$ , for the wild-type peptide, and  $(1.87 \pm 0.07) \times 10^{-6} \,\mathrm{cm^2 \, s^{-1}}$  for the citrullinated one. For comparison, the measured value of D for the reference compound dioxane was  $(1.013 \pm 0.006) \times$ 10<sup>-5</sup> cm<sup>2</sup> s<sup>-1</sup>; then, assuming its hydrodynamic radius to be 2.12 Å, the estimated hydrodynamic radii were 10.2  $\pm$  0.8 Å and 10.2  $\pm$  0.9 Å for the wild-type and citrullinated species, respectively. Thus, the two peptides had the same size in solution. These values of  $R_h$  were similar to the expected theoretical value (Danielsson et al., 2002) for a random-coil polypeptide with the same molecular weight (1985.35 Da for the wild-type and 1986.35 Da for the citrullinated species), that is,  $12 \pm 2$  Å.

To further confirm the disordered nature of the Ala21-Lys36 peptides, we also carried out homonuclear 2D-1H-NMR experiments (Tables S1 and S2). Both peptides were found to be mainly disordered in solution, supporting the far-UV CD results, as suggested by two lines of evidence. First, the sequence-corrected conformational shifts  $(\Delta \delta)$  of H<sub>\alpha</sub> protons (Cavanagh et al., 1995; Kjaergaard et al., 2011; Kjaergaard & Poulsen, 2011) were within the commonly accepted range for random-coil peptides ( $\Delta \delta \leq 0.1$  ppm) (Tables S1 and S2). And second, no long- or medium-range NOEs were detected, but only sequential ones, that is,  $\alpha N$  (i, i + 1) and  $\beta N$  (i, i + 1)(Figure 2, left side).

For the citrullinated peptide, the changes in chemical shifts were all located around the side chain corresponding to arginine in the wild-type sequence, whereas the rest of the amino acids were not affected by the modification.

Taken together, all the experimental techniques concurred to indicate that the Ala21-Lys36 peptides were monomeric (i.e., no significant self-association was observed) and disordered in aqueous solution.

# 2.1.2 | Binding of Ala21-Lys36 series peptides to PADI4

We measured the affinity of both Ala21-Lys36 peptides for PADI4 in vitro, by using three techniques. We carried out fluorescence titrations, BLI, and ITC experiments to quantitatively measure the thermodynamic binding parameters.

The fluorescence results provided a dissociation constant,  $K_d$ , for the wild-type peptide of  $9 \pm 2 \mu M$  (Table 1 and Figure 3a), whereas that of the citrullinated peptide was  $20 \pm 9 \mu M$  (Figure S2a). That is, the two values overlap within the error, but the best estimate of the dissociation constant was slightly larger for the modified peptide.

We also used ITC to assess the interaction between Ala21-Lys36 peptides and PADI4 and, therefore, to

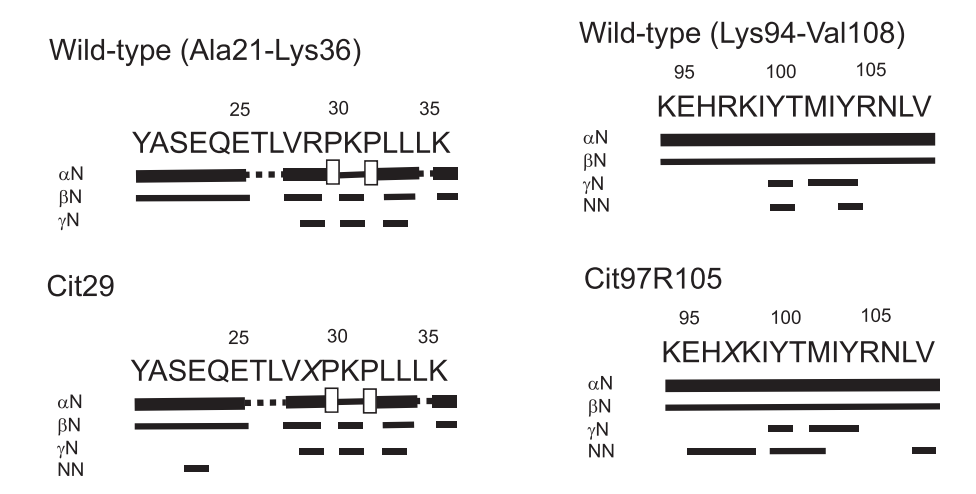


FIGURE 2 NOE diagrams of the Ala21-Lys36 and Lys94-Val108 peptide series in aqueous solution: On the left side, the NOE diagrams of the Ala21-Lys36 series are shown; in the right side, the NOE diagrams of Lys94-Val108 peptide series are shown for those peptides where assignments were possible. NOEs are classified as strong, medium, or weak, and represented by the height of the bar underneath the sequence; signal intensity was judged from the NOESY experiments. The dotted lines indicate NOE contacts that could not be unambiguously assigned. A white square indicates an  $\alpha\delta(i,i+1)$  NOEs involving a proline residue. The modified arginine in each of the series appears as "X" in the diagrams.

.wiley.com/doi/10.1002/pro.70033 by Universidad Miguel Hernández De Elche, Wiley Online Library on [29/10/2025]. See the Terms and Conditions (https:

ons) on Wiley Online Library for rules of use; OA articles are governed by the applicable Creative Commons

TABLE 1 Affinity (binding equilibrium reaction) measurements of Ala21-Lys36 or Lys94-Val108 series as determined by ITC and fluorescence (at 25°C).

	ITC <sup>a</sup>			
Peptide	$K_{\rm d}$ ( $\mu$ M)	ΔH (kcal/mol)	Fluorescence (μM) <sup>b</sup>	
Wild-type (R29)	2.9	0.9	9 ± 2	
Cit29	22	2.7	$20 \pm 9$	
Wild-type (R97R105)	1.9	2.3	$25 \pm 10 \ \mu M$	
Cit97R105	17	1.1	$20 \pm 12~\mu\text{M}$	
R97Cit105	9.4	1.0	_c	
Cit97Cit105	_d	_d	_c	

<sup>&</sup>lt;sup>a</sup>Errors are from non-linear least-squares fitting of the binding isotherm to a single binding site model.

determine the thermodynamic binding parameters of both reactions. An entropically driven endothermic interaction was observed for both peptides (Figure 3b, Figure S3, and Table 1). In all cases,  $K_d$  was in the micromolar range, exhibiting the most favorable affinity for the unmodified peptide ( $K_d = 2.9 \mu M$  for the wild-type peptide, compared to 22 µM for the citrullinated one), with a positive binding enthalpy (0.9 kcal/mol for the wild-type peptide, compared to 2.7 kcal/mol for the citrullinated one). For both peptides, the stoichiometry of the reaction was close to 2.0 moles of the peptide to 1.0 mol of dimeric PADI4, indicating that each peptide (either wild-type or citrullinated) was bound to the active site of each protomer of PADI4. Therefore, it can be concluded that the dimeric protein has two identical and independent binding sites. The addition in solution of GSK484, a competitive PADI4 inhibitor that binds to the enzyme active site, abolished the binding of both peptides from this series. The value of the IC<sub>50</sub> for GSK484 is  $\sim$ 50 nM (Lewis et al., 2015; Mondal & Thompson, 2019).

The results from BLI (Table 2) indicated that the dissociation constant, obtained from the ratio of  $k_{\rm off}$  and  $k_{\rm on}$ , was similar to those obtained by fluorescence for the wild-type peptide, thus suggesting that the two-state kinetic model assumed for the binding reaction was appropriate, although we cannot rule out other more complex processes affecting the kinetics. We could not obtain the dissociation constant from the kinetic parameters for the citrullinated peptide because a negative y-axis intercept from the pseudo-first-order plot was observed (Figure 3d). On the other hand, the association rate constant,  $k_{\rm on}$ , was similar for both peptides.

It is important to indicate (Figure 3c) that the sensorgrams showed a linear slope together to the exponential section of the curve. This linear variation, which is also observed in kinetic processes followed by other additional techniques, such as stopped-flow (Serrano

et al., 1992), could be due, among other reasons, to unspecific binding to the biosensor, as it has been suggested in other examples (Weeramange et al., 2020) (alternatively, in stopped-flow experiments the slope observed at the longest times can be due to photolysis of the reagents). The presence of such slope does not invalidate the calculation of the  $k_{\rm obs}$  in the first exponential section of the association curve; furthermore, for both peptides at any concentration, the values of the slopes ranged from 1 to  $5 \times 10^{-6} \, {\rm s}^{-1}$ . The same behavior in BLI sensorgrams was observed for the other peptide series (Section 2.2.2).

# 2.2 | Conformational features and binding to PADI4 of the Lys94-Val108 peptide series

# 2.2.1 | Conformational features of isolated Lys94–Val108 peptides

In contrast to the two peptides constituting the Ala21-Lys36 series, which had a tyrosine residue added at the N terminus, the peptides of the Lys94-Val108 series had an intrinsic fluorescence due to the presence of two tyrosine residues in their native sequence. The fluorescence spectra of each of the Lys94-Val108 peptides (the wild-type, the two single mutants, and the double mutant, Section 4.3) had a maximum around 308 nm, due to the signal of these two tyrosine residues. As in the Ala21-Lys36 series, the presence of one or two citrullinated residues (Arg97 and Arg105) did not alter the fluorescence signal. The far-UV CD spectra of the wild-type and the Cit97R105 peptides were similar to those of the Ala21-Lys36 series, with global minima around 200 nm (Figure S4), indicating that both peptides were disordered in solution. It is interesting to note that the peptide

<sup>&</sup>lt;sup>b</sup>Errors are from data fitting to Equation (1) (Section 4.4.2) or to a simplified equation obtained by Taylor expansion:  $F = F_0 + (\Delta F_{\text{max}} [\text{peptide}]_T / ([\text{peptide}]_T + K_d))$ .

<sup>&</sup>lt;sup>c</sup>Not determined because the fluorescence titrations did not show a hyperbolic behavior.

<sup>&</sup>lt;sup>d</sup>Not determined because no interaction was observed in the binding isotherm.

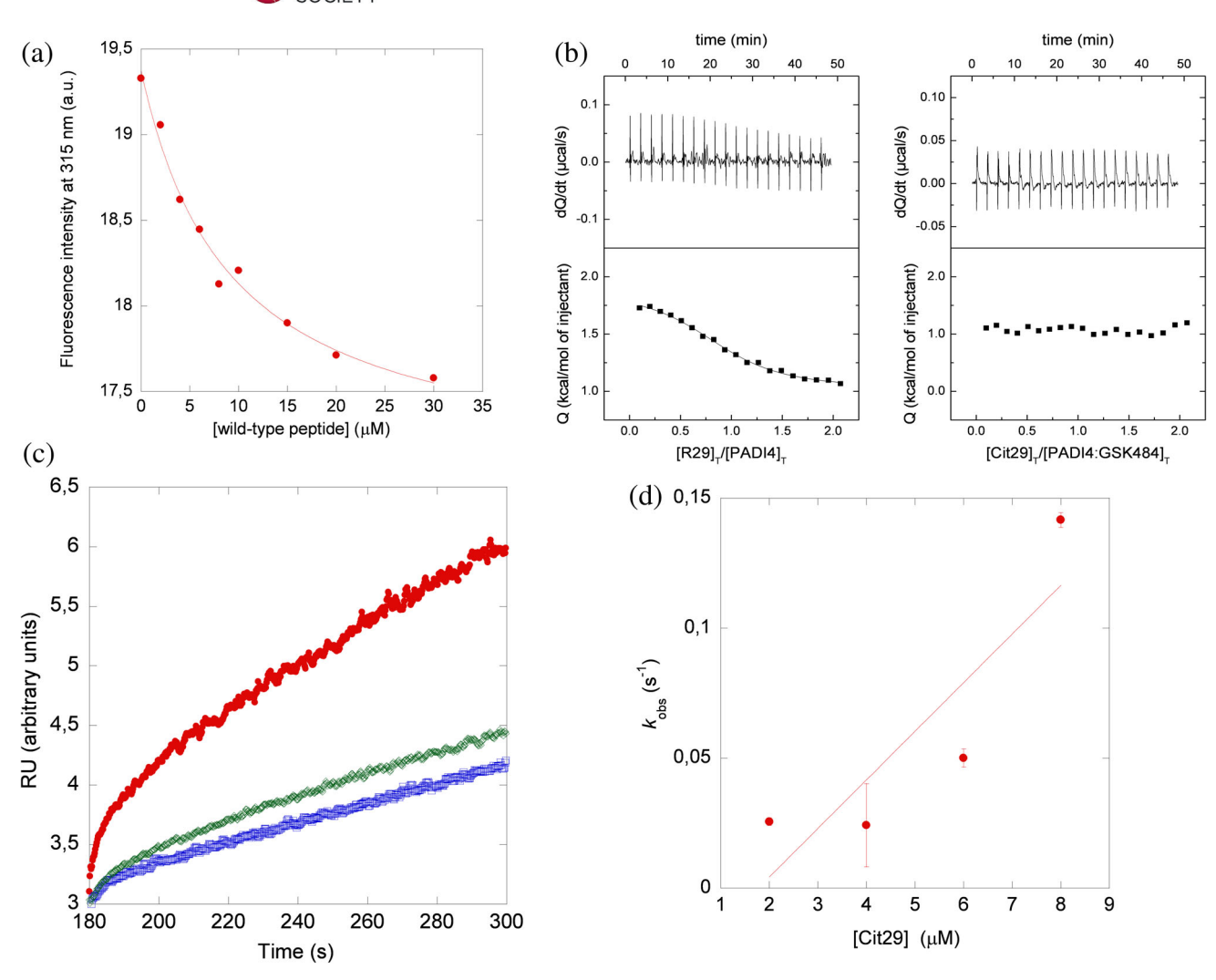


FIGURE 3 Binding of Ala21–Lys36 peptides to PADI4 as monitored by biophysical probes: (a) Titration curve monitoring the changes in the fluorescence at 315 nm when the wild-type peptide was added to PADI4. The fluorescence intensity is the relative signal after the removal of the corresponding blank. The line throughout the data is the fitting to Equation (1) (Section 4.4.2). (b) Calorimetric titrations for PADI4 binding to the wild-type peptide in the absence (left side) and presence of GSK484 (right side). Upper panels show the thermograms (thermal power as a function of time), and lower panels show the binding isotherms (ligand-normalized heat effects per injection, as a function of the molar ratio in the calorimetric cell). Continuous lines correspond to the fitting curves according to a single-ligand binding site interaction model. (c) Sensorgrams of citrullinated peptide, Cit29, at different concentrations (in colors), in the assays with PADI4 immobilized on the sensor. (d) Pseudo-first-order plot of the binding of peptide Cit29 to PADI4 (Equation 5, Section 4.9.2). The error bars are errors from fitting sensorgrams to Equation (4) (Section 4.9.2); the regression coefficient of the straight line was 0.87. Experiments were carried out at 25°C.

Cit97R105 showed a broader minimum than that observed in the spectrum of the wild-type sequence (Figure S4). However, the far-UV CD spectra of the peptides R97Cit105 and Cit97Cit105 were different, with a single, deep minima at  $\sim$ 220 nm (Figure S4); these spectra are characteristic of aggregated species or  $\beta$ -sheet conformations (Kelly et al., 2005).

The disordered character of the Lys94-Val108 peptides was further confirmed by the 1D-<sup>1</sup>H-NMR spectra of both the wild-type species (Figure 1c) and of the peptide Cit97R105, as the latter was similar to that of the

wild-type. The spectra showed a clustering of the signals of all the amide protons between 8.0 and 8.6 ppm, whereas the methyl protons were observed between 0.8 and 1.0 ppm (Figure S1b). All these values are typical of disordered polypeptide chains (Cavanagh et al., 1995). The other two peptides, namely, the peptide R97Cit105 and Cit97Cit105, had very broad 1D-¹H-NMR spectra, probably indicating the formation of soluble aggregates (data not shown); this broadening of the signals also precluded the acquisition of DOSY and of 2D-¹H-NMR spectra.

TABLE 2 Kinetic parameters of the binding reaction of the Ala21-Lys36 and Lys94-Val108 peptides to PADI4 (at 25°C).

Peptide	$k_{ m on} \ (\mu { m M}^{-1} \ { m s}^{-1})^{ m a}$	$k_{\rm off}({ m s}^{-1})^{ m a}$	$K_d$ ( $\mu$ M) (= $k_{ m off}/k_{ m on}$ ) <sup>b</sup>
Wild-type Ala21-Lys36 (R29)	$0.019 \pm 0.002$	$0.0394 \pm 0.0004$	$2 \pm 0.4$
Cit29	$0.018 \pm 0.007$	_c	_c
Wild-type Lys94-Val108 (R97R105)	$0.06 \pm 0.01$	$0.03 \pm 0.06$	$0.5 \pm 0.2$
Cit97R105	$0.03 \pm 0.01$	$0.28 \pm 0.05$	$8 \pm 3$
R97Cit105	$0.023 \pm 0.004$	$0.15 \pm 0.02$	$6 \pm 3$
Cit97Cit105	$0.042 \pm 0.005$	_c	_c

<sup>&</sup>lt;sup>a</sup>Errors are from fitting to Equation (5) (Section 4.9.2).

The D values measured by the DOSY experiment were  $(2.33 \pm 0.09) \times 10^{-6}$  and  $(2.12 \pm 0.08) \times 10^{-6}$  cm<sup>2</sup> s<sup>-1</sup> for the wild-type peptide and Cit97R105, respectively; these values were slightly larger than those measured for the Ala21-Lys36 series, probably due to: (i) the smaller number of residues in the corresponding sequences (15 residues for the Lys94-Val108 peptides compared to 17 for the Ala21-Lys36, including the additional N-terminal Tyr residue); and (ii) the more hydrophobic sequence of the Ala21–Lys36. The experimental value of D for dioxane in this case was  $(1.05 \pm 0.02) \times 10^{-5}$  cm<sup>2</sup> s<sup>-1</sup>; then, assuming again a hydrodynamic radius of 2.12 Å, the corresponding ones for wild-type and Cit97R105, respectively were  $9.5 \pm 0.9$  and  $10.5 \pm 0.8$  Å. Thus, the two radii overlapped, within the error. These values of  $R_h$  were also comparable to that obtained theoretically (Danielsson et al., 2002) for a random-coil polypeptide with the same molecular weight (1964.36 Da for the wild-type and 1965.35 Da for the citrullinated species), that is, 11.9 + 2 Å, although the experimental values corresponded to slightly more compact conformations.

To further confirm the disordered nature of the Lys94-Val108 peptides, we also carried out homonuclear 2D-<sup>1</sup>H-NMR experiments for the wild-type Cit97R105 peptides (Tables ST3 and ST4). Both peptides were mainly disordered in solution, as suggested by two lines of evidence, further confirming the results from far-UV CD (Figure S3) and 1D-1H-NMR spectra. First, the sequence-corrected conformational shifts ( $\Delta\delta$ ) of H<sub>\alpha</sub> protons (Cavanagh et al., 1995; Kjaergaard et al., 2011; Kjaergaard & Poulsen, 2011) for the assigned residues were within the commonly accepted range for randomcoil peptides ( $\Delta \delta \leq 0.1$  ppm). And second, no long- or medium-range NOEs were detected, but only sequential ones (Figure 2, right side), as it had already been observed for the Ala21-Lys36 peptides (Figure 2, left side).

Taken together, all the experimental techniques concurred to indicate that the wild-type and Cit97R105

peptides were monomeric (i.e., with no significant self-association at the concentration range explored) and disordered in aqueous solution. The far-UV CD spectra of R97Cit105 and Cit97Cit105 also suggested that also these two peptides were mainly disordered, although they had a tendency to form soluble aggregates in solution.

# 2.2.2 | Binding of Lys94–Val108 peptides to PADI4

We measured in vitro the affinity of all Lys94–Val108 peptides for PADI4, by following a three-part experimental approach. We carried out fluorescence, BLI, and ITC experiments to quantitatively measure the thermodynamic parameters of such binding.

149896x, 2025, 2, Downloaded from https://onlinelbrary.wiley.com/doi/10.1002/pro.70033 by Universidad Miguel Herrández De Elche, Wiley Online Library on [29/10/2025]. See the Terms and Conditions (https://onlinelbrary.wiley.com/errs-and-conditions) on Wiley Online Library for rules of use; O. A articles are governed by the applicable Certain Commons in the Common of the Common

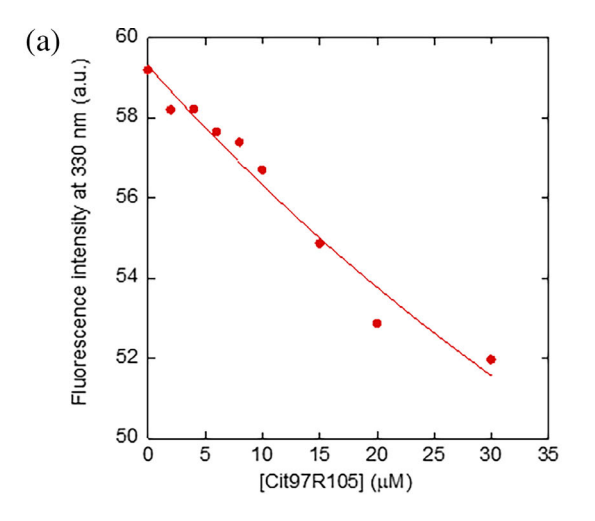
The binding reaction of wild-type to PADI4, monitored by fluorescence, yielded a dissociation constant of  $25 \pm 10~\mu M$  (Figure S2b), which was larger (corresponding to a lower affinity) than that of the wild-type of the Ala21–Lys36 series (Table 1). The binding reaction of the modified Cit97R105 yielded a dissociation constant of  $20 \pm 12~\mu M$  (Figure 4a), which was similar, within the experimental uncertainty, to that of the wild-type of this series. Attempts to determine the affinity of peptides R97Cit105 and Cit97Cit105 by fluorescence yielded unrealistically high values of  $K_{\rm d}$ , although we observed a decrease in the corrected fluorescence intensity (obtained by removing the buffer contribution) as the corresponding peptide concentration was increased (data not shown).

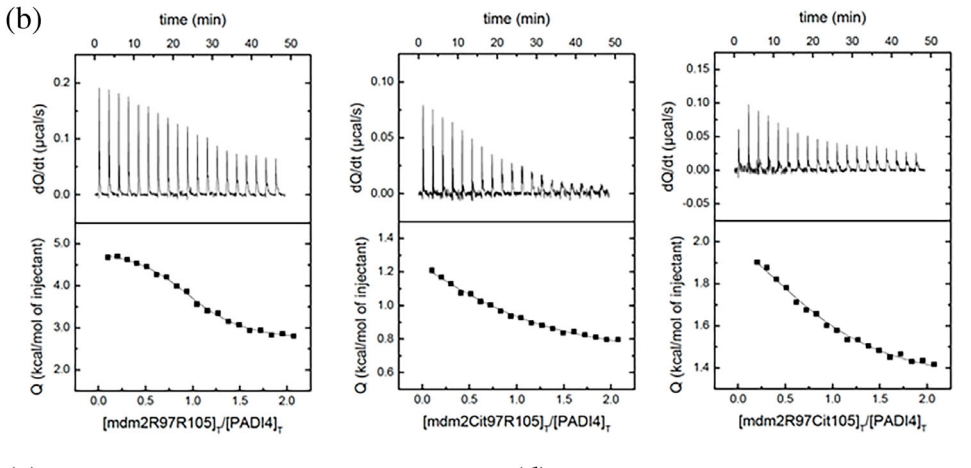
We also used ITC to estimate the thermodynamic binding parameters for the association of the peptides of the Lys94–Val108 series to PADI4 (Figure 4b). In all cases, the stoichiometry of the reaction was close to 2.0 moles of peptide to 1.0 mol of dimeric PADI4, indicating that each peptide was bound to each active site of each protomer of PADI4 (i.e., the protein dimer contains two identical and independent binding sites). Again, an

<sup>&</sup>lt;sup>b</sup>Errors are calculated as propagation errors.

<sup>&</sup>lt;sup>c</sup>Not determined because the y-axis intercept of the pseudo-first-order line was negative.

rary.wiley.com/doi/10.1002/pro.70033 by Universidad Miguel Hernández De Elche, Wiley Online Library on [29/10/2025]. See the Terms





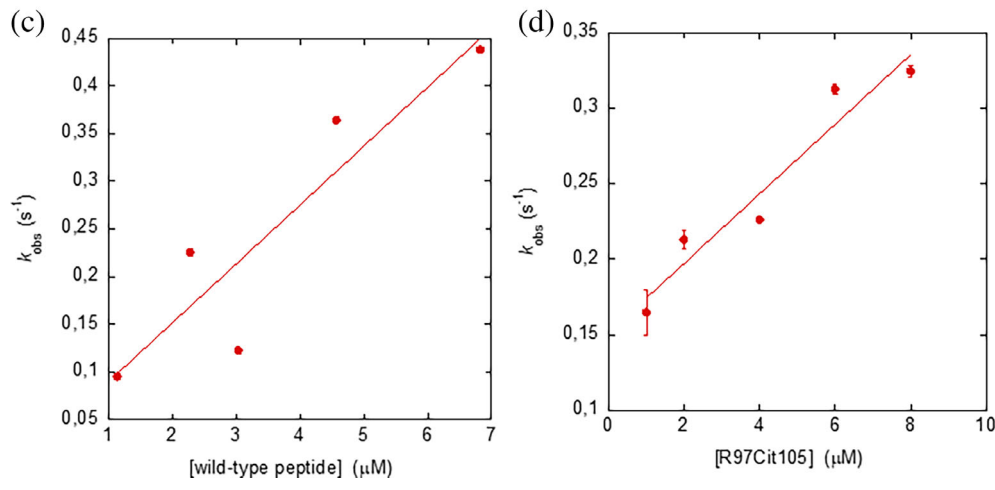


FIGURE 4 Binding of Lys94-Val108 peptide series to PADI4 as monitored by biophysical probes: (a) Titration curve monitoring the changes in the fluorescence at 330 nm when the modified peptide Cit97R105 was added to PADI4. The fluorescence intensity on the y-axis is the relative signal after removal of the corresponding blank. The line throughout the data is the fitting to Equation (1) (Section 4.4.2). (b) Calorimetric titrations for PADI4 binding to the wild-type and the two singly-citrullinated peptides. Upper panels show the thermograms (thermal power as a function of time), and lower panels show the binding isotherms (ligand-normalized heat effects per injection, as a function of the molar ratio in the calorimetric cell). Continuous lines correspond to the fitting curves according to a single-ligand binding site interaction model. Pseudo-first order plots of the binding of the (c) wild-type peptide and (d) Cit97R105 peptide (Equation 5, Section 4.9.2). The error bars are errors from fitting sensorgrams to Equation (4) (Section 4.9.2). Experiments were carried out at 25°C.

entropically driven endothermic interaction was observed for all peptides (Figure 4b and Table 1). In all cases, the dissociation constant,  $K_{\rm d}$ , was in the micromolar range, exhibiting the highest affinity for the unmodified peptide ( $K_{\rm d}=1.9~\mu{\rm M}$  for the wild-type peptide, compared to 17 and 9.4  $\mu{\rm M}$  for the singly-citrullinated peptides, Cit97R105 and R97Cit105, respectively), with a positive binding enthalpy (2.3 kcal/mol for the wild-type peptide, compared to 1.1 kcal/mol and 1.0 for the singly-

citrullinated peptides Cit97R105 and R97Cit105, respectively). Similar to the peptides from the first series, the presence of GSK484, a competitive PADI4 inhibitor that binds to the enzyme active site, abolished the binding of all peptides. The binding of the double mutant peptide (Cit97Cit105) could not be analyzed; that is, we did not observe any heat release by ITC (i.e., it was not significantly different from a control experiment consisting of injecting the peptide into buffer), and the binding

isotherm was flat with no defined trend (Figure S5). This is probably very likely due to the aggregation propensity of this peptide (Section 2.2.1). The fact that we did not observe interaction in the ITC experiments does not mean there was not binding, because (i) we observed sensorgrams in the BLI assay for this peptide (see next paragraph) from which we were able to obtain a  $k_{\rm on}$  rate for the association to PADI4; and (ii) although we could not obtain a dissociation constant from fluorescence measurements, we detected a decrease of fluorescence as the concentration of the peptide was raised.

The results from BLI measurements for the Lys94-Val108 peptides (Table 2, Figure 4c) indicated that the dissociation constant, obtained from the ratio of the  $k_{\rm off}$  and  $k_{\rm on}$ , was slightly different to that obtained by fluorescence; this finding suggests that the use of the kinetic two-state approach was not reliable for this peptide series. The apparent  $K_d$  obtained from the kinetic data was larger for the citrullinated peptides than for the wild-type (Table 2), but it must be kept in mind that these  $K_d$  values were obtained by assuming a two-step process for the peptide binding, which at this stage was not fully proved. The  $k_{\rm on}$  rates were similar among the four peptides (0.04  $\mu M^{-1} s^{-1}$  on average), but the  $k_{\rm off}$  rates were larger for the citrullinated peptides than for the wild-type one, that is, the modified peptides dissociated faster from PADI4 (and therefore their  $K_d$  values were larger). The kinetic rates were very different between the Ala21-Lys36 and Lys94-Val108 series.

# 2.3 | Molecular simulations of the PADI4-peptides interface

# 2.3.1 | All the peptides target the catalytic sites of PADI4

To investigate at atomic detail the binding region of our peptides to PADI4, we used molecular docking. This technique is difficult to apply to peptides because they have a high conformational versatility that should be taken into account in simulation. In fact, although in principle any predictor for protein–protein complexes can also be used to model a protein–peptide complex, in practice, this would lead to bound peptide conformations that mostly resemble the unbound structure given as an input. On the other hand, any traditional algorithm for the docking of small compounds could equally be used, but with a low reliability due to the large number of degrees of freedom in the molecular system (>70 dihedral angle rotations in our peptides). However, novel and more efficient docking software is currently being

explored that could represent a step forward in this direction.

In this context, we have used our peptides as a test case for DiffDock (Corso et al., 2022), one of the most promising algorithms currently under development (Isert et al., 2023), which treats the docking process as a diffusion generative model over the (non-Euclidean) manifold of ligand poses. The results obtained by using this methodology showed that all our peptides, including the two wild-type sequences and all their variants in citrullinated form, diffused towards the catalytic site of PADI4 as their binding target. Figure 5 reports as an example the three most favorable docking poses obtained for each peptide, although we note that all the binding modes (40 for each simulation) converged toward the protein catalytic region.

These results strongly suggest that all the peptides bind to the orthosteric site that PADI4 employs to interact with its natural substrates. Furthermore, it indicates that the binding of the peptides to (putative) allosteric or unspecific sites on the protein surface is negligible or null. These findings are also in agreement with the indication of our ITC experiments showing that the enzymatic PADI4 inhibitor GSK484, which is known to bind to the catalytic site, blocks the association of the ligands to this protein.

Unfortunately, and probably due to the computational complexity in the binding of our peptides (which are relatively large compared to the typical compounds being currently tested in the development of DiffDock (Corso et al., 2022)), we also observed local steric clashes in the bound conformations predicted by this algorithm. Therefore, the specific binding poses obtained were not analyzed in details and a more accurate docking algorithm was further used (see below), distinctively tailored for predicting protein–peptide interactions.

# 2.3.2 | Predicted key residues involved in the PADI4–peptides binding

To further investigate the binding of our peptides to PADI4, we used MDockPeP (Xu & Zou, 2020), an algorithm that is specifically intended to predict protein-peptide complexes. In spite of its accuracy, MDockPeP has some restrictions compared to algorithms developed for docking small compounds, including DiffDock (see above). First, it is limited to protein targets having a maximum of 1000 amino acid residues, therefore restraining our possibility of use to the sole monomeric species of PADI4 (663 residues). A second restriction is that the peptide sequence cannot include a non-standard amino acid such as citrulline, therefore limiting our simulations

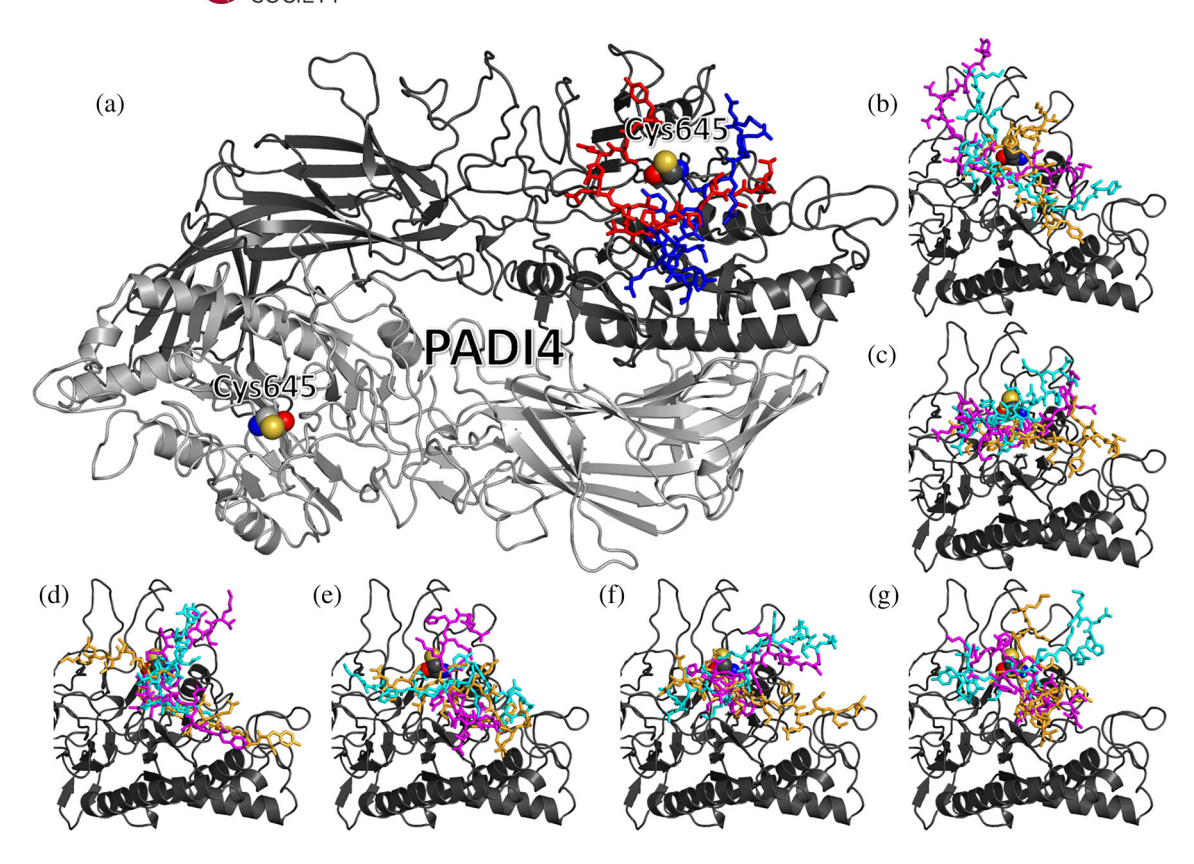


FIGURE 5 Binding of both peptide series to PADI4 as monitored by in silico experiments: (a) Homodimeric structure of PADI4 with the best docking pose obtained by DiffDock for the wild-type peptides (red) Ala21–Lys36 and (blue) Lys94–Val108, bound to the same monomer; the key catalytic residues Cys645 are also labeled. (b)–(g) Details of the binding site of PADI4, slightly rotated with respect to the view shown in (a). The three most favorable docking poses (1st: magenta; 2nd: cyan; 3rd: yellow) predicted by DiffDock are shown for all the peptides: (b) wild-type Ala21–Lys36, (c) wild-type Lys94–Val108, (d) Cit29, (e) Cit97R105, (f) R97Cit105, and (g) Cit97Cit105.

to the sole wild-type peptides. A third, minor constraint is that the peptide sequences could include a maximum of 15 residues. This was sidestepped by eliminating the first and last residue in the simulation of the peptide Ala21–Lys36 (the first residue being the additional N-terminal tyrosine that is not part of the wild-type MDM2 sequence), whereas the length of peptide Lys94–Val108 was within this limit. Finally, another minor restriction is that MDockPeP only allows standard peptide termini; therefore, the specific cappings present in our cases (acetylated and amidated, respectively) could not be accurately modeled.

In a first step, the ability of MDockPeP to reproduce the trend previously observed by using DiffDock was tested for the two wild-type sequences of the two series through a blind docking on the whole surface of the PADI4 monomer. For the peptide Ala21–Lys36, the three most favorable docking poses were all found in correspondence of the enzymatic site of PADI4, after eliminating the poses at the dimeric interface that would clash with the other monomer—as they could exist only in the case of dimer dissociation, which was not observed in our

wet-lab experiments. For the peptide Lys94–Val108, no docking poses were found in any position at the monomer-monomer interface, and most poses (including those ranked 1st, 2nd, and 5th in our calculation) were found to occupy the catalytic site as well.

After this initial success, the docking search of MDockPeP was restricted to the sole active site of PADI4, by considering a binding region centered on the sulfur atom of the catalytic residue, Cys645, and having a smaller size (50, 40, or 30 Å), and again the first three best poses were selected. Added up to the ones previously found, this led to a total of 12 docking poses for each peptide sequence, which were rescored by using the MM/GBSA methodology (Chen et al., 2016) for two reasons: (i) to have a more accurate estimation of the binding energy and (ii) to identify the key residues involved in the binding. Table 3 shows the results obtained for the best six poses for each peptide. The peptide Ala21-Lys36 had a lower binding affinity compared to Lys94-Val108  $(-68.5 \pm 8.2 \text{ vs} - 79.0 \pm 9.6 \text{ kcal/mol}, \text{ respectively})$ . However, the two values overlapped within their uncertainties, and the former was also affected by the absence



**TABLE 3** Docking poses of the wild-type peptides of N-MDM2 to PADI4, predicted by MDockPeP and ranked using the MM/GBSA technique, with their total binding affinity and best per-residue contribution (energies in parentheses).

Wild-type peptide	Pose rank		Best contributions to binding affinity (kcal/m	
		Binding affinity (kcal/mol)	PADI4	Peptide
Ala21-Lys36	1	-78.36	Asp632 (-10.47), Phe633 (-6.51), Thr635 (-5.62)	Leu33 (-9.45), Arg29 (-7.58), Leu34 (-6.75)
	2	-75.18	Asp632 (-11.06), Phe633 (-6.11), Phe634 (-4.73)	Leu33 (-9.24), Arg29 (-6.99), Leu34 (-6.77)
	3	<b>-72.69</b>	Asp632 (-6.65), Asp350 (-5.15), Phe633 (-5.09)	Leu34 (-8.60), Arg29 (-8.37), Gln24 (-4.63)
	4	-65.80	Phe314 (-6.51), Asn316 (-5.80), Asp632 (-5.10)	Arg29 (-8.81), Pro32 (-6.82), Gln24 (-6.33)
	5	-60.20	Phe633 (-9.55), Phe314 (-5.61), Phe634 (-4.13)	Leu33 (-7.69), Leu34 (-7.03), Gln24 (-4.31)
	6	-58.67	Ser406 (-7.69), Ile313 (-3.85), Phe633 (-3.81)	Leu34 (-7.34), Leu33 (-5.49), Ser22 (-4.03)
Lys94–Val108	1	-90.14	Asp350 (-4.62), Phe633 (-3.75), Tyr636 (-3.57)	Tyr100 (-7.45), Tyr104 (-6.02), Lys94 (-5.99)
	2	-89.47	Val469 (-6.42), Tyr636 (-4.71), Cys645 (-3.97)	Arg97 (-8.07), Tyr104 (-6.06), His96 (-4.97)
	3	-82.42	Ile313 (-6.13), Asp350 (-4.54), Tyr636 (-3.64)	Tyr100 (-7.83), Tyr104 (-7.24), His96 (-5.41)
	4	<b>-72.29</b>	Gln346 (-5.01), Asp473 (-4.35), Glu351 (-3.68)	Arg97 (-13.21), Tyr104 (-9.90), Ile99 (-5.58)
	5	-70.94	Asp632 (-7.09), Glu642 (-6.00), Arg372 (-5.19)	Thr101 (-5.55), Met102 (-4.38), Arg105 (-3.21)
	6	-68.70	Ser402 (-4.59), Asp632 (-4.27), Val469 (-3.81)	Arg97 (-7.93), Tyr100 (-5.85), His96 (-5.60)

of the two terminal residues that could not be included in the calculations.

From a structural point of view, the docking ensemble of the two peptides appeared fuzzy (Figure S6). We also note that the binding modes predicted for both wild-type peptides appeared more compact compared to the ones previously obtained by using DiffDock (Figure 5), possibly due to a better convergence of the MDockPeP algorithm toward more accurate docking poses on the surface topography of PADI4. Therefore, the docking poses previously obtained by using DiffDock are likely

more representative of the first steps of the formation of the PADI4/peptides complex. For both peptides, the binding modes predicted by MDockPeP appeared to be driven by a combination of electrostatic and hydrophobic interactions. In particular (Table 3), Arg29 was the key residue for the binding of peptide Ala21–Lys36, with the backing of non-polar interactions by the aliphatic side chains of Leu33 and Leu34. For the peptide Lys94–Val108, the most important arginine residue for the binding appeared to be Arg97, together with the aromatic rings of His96, Tyr100, and Tyr104. For PADI4, the

469896x, 2025, 2, Downloaded from https

com/doi/10.1002/pro.70033 by Universidad Miguel Hernández De Elche, Wiley Online Library on [29/10/2025]. See the Terms

conditions) on Wiley Online Library for rules of use; OA articles are governed by the applicable Creative Commons

crucial hot-spot for the binding was the region Asp632–Tyr636, in agreement with the findings we had obtained with the intact MDM2 (Araujo-Abad, Rizzuti, et al., 2023) and other molecular partners (Araujo-Abad et al., 2024).

# 2.4 | The two wild-type peptides, R29 and R97R105, were substrates of PADI4

The ITC findings in the presence of GSK484 (Figure S3) and the in silico results (Figure 5) suggest that both wild-type peptides bind to the active site of the protein. Therefore, we wondered whether the two peptides could be substrates of the enzyme and whether the citrullination could be directly observed. To that end, we used a colorimetric procedure based on the color developing reagent (COLDER) (Knipp & Vašák, 2000), which has been used to show the activity of PADI4 for other substrates (Kearney et al., 2005).

To that end, we first carried out control experiments with a solution containing 100  $\mu$ M of L-citrulline and with a well-known substrate of PADI4: N- $\alpha$ -benzoyl-L-arginine ethyl ester (BAEE) at two different concentrations, 100  $\mu$ M and 10 mM. The absorbance spectra collected between 400 and 600 nm showed that (i) the L-citrulline was modified by the COLDER agent and (ii) PADI4 purified in our laboratories was capable of modifying BAEE under our experimental conditions (Figure 6).

Next, we carried out experiments in the presence of PADI4 (0.7  $\mu$ M in protomer units) and 100  $\mu$ M of either R29 or R97R105. The spectra showed that the peptides were modified in the presence of the enzyme with the development of the same color as in the case of BAEE and L-citrulline, but with a lower final intensity of the spectrum. Furthermore, when the enzyme was not present, we did not observe any color appearing in solution (Figure 6), indicating that there was no modification in this case.

These results indicate that the wild-type peptides not only did bind to PADI4, but they were also substrates of the protein, being citrullinated in the catalytic reaction.

### 3 | DISCUSSION

We have shown that a direct interaction of intact MDM2 with PADI4 takes place through the N-terminal region of MDM2 (Araujo-Abad, Rizzuti, et al., 2023), that is, N-MDM2, which also intervenes in the interaction with the S100 proteins (van Dieck et al., 2010), p53 (Li et al., 2008; Yang et al., 2021), and the sterile alpha motif

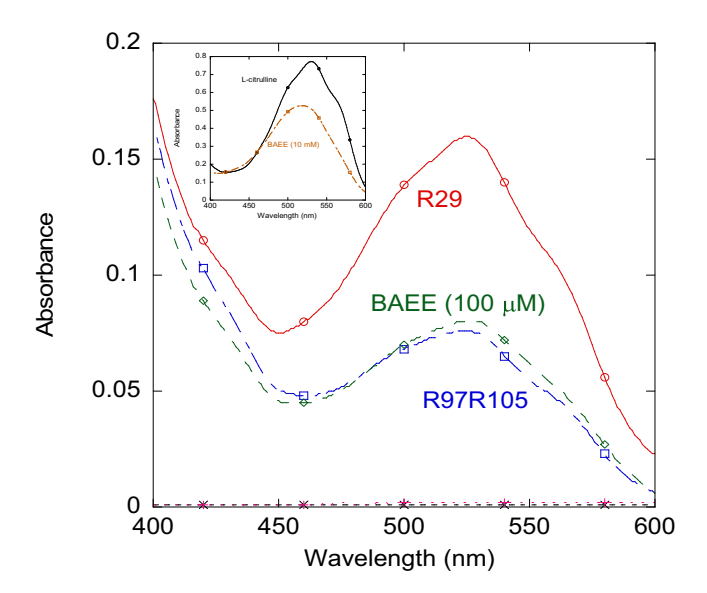


**FIGURE 6** Citrullination of the wild-type peptides of both series. Absorbance (UV) spectra of BAEE (100 μM), R29 (100 μM), and R97R105 (100 μM) after incubation with PADI4 in the presence of 10 mM  $Ca^{2+}$  (in 100 mM Tris, pH 7.6) and treatment with the color developing agent (COLDER). (Inset) To allow for a comparison in the absorbance scale (UV), the spectra of L-citrulline (100 μM), after treatment with COLDER, and that of BAEE (10 mM), after incubation with PADI4 and treatment with COLDER, are shown. The spectra close to the *x*-axis in the main panel correspond to R29 (100 μM, indicated with × symbols) and R97R105 (100 μM, indicated with + symbols) after treatment with COLDER (and no incubation with PADI4).

(SAM) of p73, SAMp73 (Neira et al., 2019). NMR mapping experiments indicate that the PADI4-binding region of N-MDM2 comprises residues Thr26, Val28, Gln44 (all involved in several protein loops), Phe91 (in the last β-strand of the sheet (Kussie et al., 1996; Uhrinova et al., 2005)), and Lys98 (at the C-terminal  $\alpha$ -helix in N-MDM2 (Araujo-Abad, Rizzuti, et al., 2023; Kussie et al., 1996; Uhrinova et al., 2005)). We have also hypothesized that Arg97 and Arg105 are the most likely candidates to be citrullinated (Araujo-Abad, et al., 2023). With the aim to show that those regions are substrates of the enzyme, in this work, we have synthesized peptides comprising Arg29, Arg97, and Arg105, as well as their citrullinated variants. We have shown that the modification at Arg29 did not alter substantially the structural features of such region. Unfortunately, we have not been able to obtain a full structural information on the conformational features of the region including Arg97 and Arg105 of N-MDM2, due to the observed aggregation of some of the corresponding isolated peptides, involving citrullination at those positions. In a previous work (Sharma et al., 2019), a peptide, comprising the PADI2-target region of RNA polymerase II, has been

used to determine the affinity of that enzyme for such polypeptide region. The results, obtained by microscale thermophoresis, yield a value of the dissociation constant of  $0.22 \pm 0.05~\mu M$  (Sharma et al., 2019), which is one order of magnitude lower (~2–3  $\mu M$ ) than the values reported in this work for the wild-type N-MDM2 peptides (Table 1). This result suggests that a "divide-and-conquer" approach, such as the one we have also employed, is useful to determine how N-MDM2 could interact with the citrullinating enzyme.

We have measured, by using ITC, that the dissociation constant of intact N-MDM2 for PADI4 is 1.0 ± 0.2 μM (Araujo-Abad, Rizzuti, et al., 2023). The values found in this work for the association of wild-type peptides to PADI4 were in the same range ( $K_d$  of 2-3  $\mu$ M, Table 2), indicating that the binding is governed mainly by residues in those peptides. In all peptides, the binding was entropically driven, with a small unfavorable enthalpy. However, the citrullination of arginines within these peptides caused a considerable reduction in the binding affinity. For the peptide citrullinated in the position 29, Cit29, the reduction stems from a more unfavorable enthalpic contribution and a less favorable entropic contribution to the Gibbs energy of binding, whereas for the peptides citrullinated at Arg97, that is, Cit97R105, or Arg105, that is, R97Cit105, the reduction in affinity stems from a less favorable entropic contribution to the Gibbs energy of binding, since the enthalpy was slightly less unfavorable.

On the other hand, for the binding of the intact N-MDM2 to PADI4, we previously obtained for the two kinetic rates the following values:  $k_{\rm on}=0.17\pm0.10~\mu{\rm M}^{-1}~{\rm s}^{-1}$  and  $k_{\rm off}=0.3\pm0.2~{\rm s}^{-1}$  (Araujo-Abad, Rizzuti, et al., 2023). The  $k_{\rm on}$  value for the intact N-MDM2 is larger than those for the peptides (Table 2), probably due to the other regions present in the protein which can assist or guide in the binding to PADI4. Moreover, the  $k_{\rm off}$  rates for the citrullinated Lys94–Val108 peptides were similar to that of the intact protein.

A comparison with the  $k_{\rm on}$  rates of Ala21–Lys36 and Lys94–Val108 series with other citrullinated peptides of PADI4 (Neira et al., 2024) does not lead to any significant conclusion, but the  $k_{\rm off}$  of the citrullinated peptides for the Lys94–Val108 series was larger (in general terms, by one order of magnitude) than those reported for the other citrullinated peptides coming from auto-citrullination of PADI4 (Neira et al., 2024). Thus, it seems that the values of both kinetics rates are strongly sequence-dependent.

The disordered nature of the N-MDM2 peptides in solution suggests that the binding to PADI4 may lead to a fuzzy complex with this protein, with a variety of possible binding conformations within the same binding site. The docking simulations confirmed this hypothesis,

indicating the catalytic site of PADI4 as the hot-spot for the binding, in agreement with the ITC experiments showing that the association is blocked by the competitive binding of the selective inhibitor GSK484. In particular, the key region of PADI4 in the anchoring is predicted to be the protein patch Asp632–Tyr636, which we had already observed is crucial for the binding in vivo with intact MDM2 (Araujo-Abad, Rizzuti, et al., 2023), and RING1B (Araujo-Abad et al., 2024). The simulations also suggest that the peptides rely for the binding not only on the Coulombic contribution of their arginines residues (for both wild-type species), but also on hydrophobic interactions with the aliphatic side chains of leucines (for the Ala21–Lys36 species) or tyrosines (for the Lys94–Val108 peptides).

Finally, we have also shown, by using a spectrophotometric reaction, that both wild-type peptides are substrates of PADI4. Therefore, they could also be considered as a reference to develop novel peptide inhibitors to target PADI4 (possibly after some improvements to restrict their flexibility), enlarging in this way the range of possibilities to drug-target this enzyme.

### 4 | MATERIALS AND METHODS

### 4.1 | Materials

Imidazole, Trizma base, DNase, SIGMAFAST protease tablets, BAEE, L-citrulline, hydroxyimino 2-butanone (DAMO), thiosemicarbazide (TSC), SO<sub>4</sub>H<sub>2</sub> (96–98%), PO<sub>4</sub>H<sub>3</sub> (85%), NH<sub>4</sub>Fe(SO<sub>4</sub>)<sub>2</sub>·12 H<sub>2</sub>O, NaCl, Ni<sup>2+</sup>-resin, 3-(trimethylsilyl) propionic acid-2,2,3,3-2H<sub>4</sub>-sodium salt (TSP), deuterated Tris acid, Amicon centrifugal devices with a molecular weight cut-off of 50 kDa, and ultra-pure dioxane were all purchased from Sigma-Merck (Madrid, Spain). The β-mercaptoethanol was from BioRad (Madrid, Spain). Ampicillin and isopropyl-β-L-1-thiogalactopyranoside were obtained from Apollo Scientific (Stockport, UK). Triton X-100, tris(2-carboxyethyl) phosphine (TCEP) Cavanagh and the SDS protein marker (PAGEmark Tricolor) were from VWR (Barcelona, Spain). The rest of the materials used were of analytical grade. Water was deionized and purified on a Millipore system.

## 4.2 | Protein expression and purification

PADI4 was purified in its dimeric form as previously described (Araujo-Abad et al., 2024; Araujo-Abad, Fuentes-Baile, et al., 2023; Araujo-Abad, Rizzuti, et al., 2023; Neira et al., 2024; Neira, Araujo-Abad,

et al., 2022; Neira, Rizzuti, et al., 2022). Protein concentration was determined by UV absorbance, employing an extinction coefficient at 280 nm estimated from the 10 tryptophans and 13 tyrosines *per* monomer  $(73,540 \text{ M}^{-1} \text{ cm}^{-1})$  (Gill & von Hippel, 1989).

# 4.3 | Peptide design

All peptides were synthesized and purified by GenScript (Amsterdam, Netherlands) and had the N terminus acetylated and the C terminus amidated. The sequences were as follows:

(a) The Ala21-Lys36-region series: The peptides were (R29): YA<sup>21</sup>SEwild-type peptide QETLVRPKPLLLK<sup>36</sup> and (ii) the peptide with the Arg29 modified (Cit29) to citrulline (indicated as an X in the following sequences) YA<sup>21</sup>SEOETLVXPKPLLLK<sup>36</sup>. For both peptides, the tyrosine residue at the N terminus (Y<sup>20</sup>) was added to allow for an accurate peptide quantification by using absorbance. We did not include a tryptophan to help measure the absorbance, instead of the chosen tyrosine, due to (i) its larger, more hydrophobic side-chain, compared to that of tyrosine; and (ii) the possibility of a more significant interference of such aromatic indole moiety on the far-UV CD of the isolated peptides (Kelly et al., 2005; Vuilleumier et al., 1993).

(b) The Lys94–Val108–region series: The peptides were (i) the wild-type peptide (R94/R105):  $K^{94}EHRKIYT-MIYRNLV^{108}$ ; (ii) the single citrullinated peptides: (Cit94)  $K^{94}EHXKIYTMIYRNLV^{108}$ , and (Cit105)  $K^{94}EHRKIYTMIYXNLV^{108}$ ; and (iii) the double modified peptide (Cit94Cit105)  $K^{94}EHXKIYTMIYXNLV^{108}$ .

Peptide concentration for both series was determined by UV absorbance, employing the extinction coefficient of the single tyrosine in the peptides of the Ala21–Lys36 series and the two tyrosines in the Lys94–Val108 series (Gill & von Hippel, 1989).

### 4.4 | Fluorescence

## 4.4.1 | Steady-state fluorescence

Fluorescence spectra were collected on a Cary Varian spectrofluorometer (Agilent, Santa Clara, CA, USA), interfaced with a Peltier unit. Following the standard protocols used in our laboratories, the samples were prepared the day before and left overnight at 5°C; before experiments, samples were left for 1 h at 25°C. A 1-cm-pathlength quartz cell (Hellma, Kruibeke, Belgium) was used. Concentration of PADI4 was 2  $\mu$ M (in protomer units), and that of the corresponding peptide was 20  $\mu$ M.

Experiments were performed in 20 mM Tris buffer (pH 7.5), 5 mM TCEP, 150 mM NaCl, and 5% glycerol. Protein samples were excited at 280 and 295 nm, to follow the fluorescence of both tyrosine and tryptophan residues (280 nm) or only that of tryptophan (295 nm). The other experimental parameters have been described elsewhere (Araujo-Abad, Fuentes-Baile, et al., 2023). Appropriate blank corrections were made in all spectra. Fluorescence experiments were repeated in triplicates with newly prepared samples. Variations of results among the experiments were lower than 10%.

## 4.4.2 | Binding experiments with PADI4

For the titration between the peptides of either the Ala21-Lys36 or Lys94-Val108 series and PADI4, increasing amounts of the corresponding peptide, in the concentration range 0-30 µM, were added to a solution with a fixed concentration of PADI4 (2.0 µM in protomer units). The samples were prepared the day before and left overnight at 5°C; before the measurements, they were incubated for 1 h at 25°C. Experiments were carried out in the same buffer used for the steady-state experiments. The samples were excited at 280 and 295 nm, and the rest of the experimental set-up was the same described above. In all cases, the appropriate blank corrections were made by subtracting the signal obtained with the corresponding amounts of the Ala21-Lys36 and Lys94-Val108 peptide series by using the software KaleidaGraph (Synergy software, Reading, PA, USA). Spectra were corrected for inner-filter effects during fluorescence excitation (Birdsall et al., 1983). The titration was repeated three times, by using new samples; variations in the results were lower than 10%.

The dissociation constant of the corresponding complex,  $K_d$ , was calculated by fitting the binding isotherm constructed by plotting the observed fluorescence change as a function of peptide concentration to the general binding model, explicitly considering polypeptide depletion due to binding (Beckett, 2011; Royer & Scarlata, 2008):

$$\begin{split} F &= F_0 + \frac{\Delta F_{max}}{2[PADI4]_T} \left( [\text{peptide}]_T + [\text{PADI4}]_T + K_d \right) \\ &- \sqrt{\left( \left( [\text{peptide}]_T + [\text{PADI4}]_T + K_d \right)^2 - 4[\text{peptide}]_T [\text{PADI4}]_T \right)}, \end{split}$$

where F is the measured fluorescence at any particular concentration of the peptide after subtraction of the spectrum of sample containing only the same concentration of such protein (i.e., F is the difference fluorescence after

blank subtraction);  $\Delta F_{\rm max}$  is the largest change in the fluorescence of the peptide when all polypeptide molecules were forming the complex, compared to the fluorescence of each isolated polypeptide (at the same corresponding concentration);  $F_0$  is the fluorescence intensity when no peptide was added;  $[PADI4]_T$  is the constant, total concentration of PADI4 (2.0  $\mu$ M in protomer units); and  $[peptide]_T$  is that of the corresponding Ala21–Lys36 or Lys94–Val108 series, which was varied during the titration. Fitting to Equation (1) was carried out by using KaleidaGraph.

# 4.5 | Circular dichroism (CD)

Far-UV CD spectra were collected on a Jasco J810 spectropolarimeter (Jasco, Tokyo, Japan) thermostated cell holder and interfaced with a Peltier unit. The instrument was periodically calibrated with (+)-10-camphorsulfonic acid. A cell of pathlength 0.1 cm was used (Hellma, Kruibeke, Belgium). All spectra were corrected by subtracting the corresponding baseline. The concentration of each polypeptide (both PADI4 and each of the specific N-MDM2 peptide added) and the buffers were the same used in the fluorescence experiments and, more generally, samples were prepared in the same way as in those experiments. The raw ellipticity, Θ, provided by the instrument (in mdeg) was converted to molar ellipticity,  $[\Theta]$ , defined as:  $[\theta] = \theta/(10lcN)$ , where l is the pathlength of the cell, c is the molar concentration, and N is the number of peptide bonds (which is 14 for the Lys94–Val108 series and 15 for the Ala21-Lys36 one).

Isothermal wavelength spectra of each isolated polypeptide and that of the complex were acquired as an average of 6 scans, at a scan speed of 50 nm/min, with a response time of 2 s and a band-width of 1 nm at 25°C.

# 4.6 | Nuclear magnetic resonance (NMR) spectroscopy

The NMR spectra of the isolated Ala21–Lys36 or Lys94–Val108 peptides were acquired at  $10^{\circ}$ C on a Bruker Avance 500 MHz spectrometer (Bruker GmbH, Germany), equipped with a triple resonance probe and z-pulse field gradients. Spectra were processed with Bruker TopSpin 2.1 (Bruker GmbH, Karlsruhe, Germany). The temperature of the probe was calibrated with pure methanol (Cavanagh et al., 1995). All NMR experiments with both peptide series were carried out in 50 mM  $d_{12}$ -Tris buffer corrected for isotope effects, at pH 7.2. Spectra were calibrated with TSP, by considering the

pH-dependent changes of its chemical shifts (Cavanagh et al., 1995).

# 4.6.1 | 1D-<sup>1</sup>H-NMR spectra

Around 128 scans were acquired with 16 K acquisition points for the homonuclear 1D-¹H-NMR spectra of each isolated peptide at a concentration of 1.5 mM. Water signal was suppressed with the WATERGATE sequence (Piotto et al., 1992). The spectra were processed after zero-filling and apodization was carried out with an exponential window.

# 4.6.2 | Translational diffusion NMR (DOSY)

The concentrations of both peptide series in DOSY experiments were 100 µM, and 256 scans were acquired, in which the gradient strength was varied linearly. Measurements of the translational self-diffusion coefficient were performed with the pulsed-gradient spin-echo sequence in the presence of 100% D<sub>2</sub>O. Details on the experimental conditions and the protocols of fitting of the resulting curves have been described elsewhere (Neira et al., 2016). During the acquisition, the gradient strength was varied in 16 linear steps between 2% and 95% of the total power of the gradient coil. Gradient strength was calibrated by using the value of the translational diffusion coefficient, D, for the residual proton water signal in a sample containing 100% D<sub>2</sub>O, in a 5-mm tube (Wilkins et al., 1999). In the experiments with both peptide series, the gradient length was 2.5 ms; the time between the two pulse gradients in the pulse sequence was 250 ms; and the recovery delay between the bipolar gradients was 100 us. The signals of the methyl groups between 0.8 and 1.0 ppm were used for peak integration, for both peptide series. A final concentration of 1% of dioxane, which was assumed to have a hydrodynamic radius  $R_h$  of 2.12 Å (Wilkins et al., 1999), was added to the solution to be used as a reference to measure the  $R_{\rm h}$  value.

# 4.6.3 | 2D-1H-NMR spectra

Two-dimensional <sup>1</sup>H-NMR spectra of the both peptide series were acquired in each dimension in phase-sensitive mode by using the time-proportional phase incrementation technique (Marion & Wüthrich, 2012) and a spectral width of 5500 Hz. Peptide concentration was the same used in the 1D experiments and the pH values of the samples were those reported above. Standard TOCSY (Bax and Davies, 1969) (total correlation spectroscopy),

and NOESY (nuclear Overhauser effect spectroscopy) (Kumar et al., 1980), with mixing times of 80 and 200 ms, respectively, were performed by acquiring a data matrix size of  $4096 \times 256$  points. The relaxation time in both experiments was 1 s. The DIPSI (decoupling in the presence of scalar interactions) spin-lock sequence (Cavanagh, 1992) was used in the TOCSY experiments. A number of 88 scans were acquired per increment in the first dimension, and the residual water signal was removed by using the WATERGATE sequence (Piotto et al., 1992). NOESY spectra were collected with 128 scans per increment in the first dimension, using again the WATERGATE sequence (Piotto et al., 1992). Data were zero-filled, resolution-enhanced with a square sine-bell window function optimized for each spectrum, and baseline-corrected. The <sup>1</sup>H resonances were assigned by standard sequential assignment processes (Cavanagh et al., 1995). The chemical shift values of  $H_{\alpha}$  protons in random-coil regions were obtained from comparison with the values of model polypeptides, corrected by neighboring residue effects (Cavanagh et al., 1995; Kjaergaard et al., 2011).

# 4.7 | Citrullination determination by a colorimetric assay

A photometric method used in the determination of L-citrulline was used to determine whether PADI4 was capable of citrullinating the two wild-type peptides in both series, R29 and R97R105. This method is based in the reaction of citrulline with oxymes, such as 3-hydroxyimino 2-butanone (or diacetyl monoxime) in strong acids in the presence of thiosemicarbazide (TSC). The protocol to prepare the color developed reagent (COLDER) has been described elsewhere (Knipp & Vašák, 2000) and applied to detect the enzyme activity of PADI4 (Kearney et al., 2005). We prepared stocks solutions of 0.05 M L-citrulline and 0.1 M of N-α-benzoyl-L-arginine ethyl ester (BAEE) for the control experiments to set up the conditions of the reaction.

All absorption spectra were recorded between 400 and 600 nm on UV-Visible spectrophotometer Shimadzu UV-1603 by Shimadzu (Kyoto, Japan). All spectra were acquired at room temperature. Water was used as a reference for a blank subtraction.

In the first step, we prepared a solution containing a final concentration of  $100 \mu M$  of L-citrulline up to a volume of  $500 \mu L$  in water, from the stock solution of the compound. We incubated the resulting solution at  $95^{\circ}C$  for  $15 \min$  after adding 2 mL of the color developing agent (COLDER), which was freshly prepared

as described (Knipp & Vašák, 2000). After cooling at room temperature, the samples were transferred into 1 mL-quartz cuvettes to be measured in the spectrophotometer. These control experiments were repeated twice.

In the second step, we prepared two solutions containing a final concentration of 100 µM and 10 mM of BAEE from the stock BAEE solution. The corresponding volumes from the BAEE stock solution were dissolved in the "reaction buffer" containing 100 mM Tris (pH 7.6), 50 mM NaCl, 2 mM DTT, and 10 mM CaCl<sub>2</sub> up to a final volume of 500 µL. The resulting solution was incubated for 15 min at 37°C in an Innova 4000 new Brunswick scientific incubator (Thermofisher, Madrid, Spain) with a 150 rpm shaking. After such period of time, we added PADI4 to each of the BAEE concentrations, to yield a final 0.7 µM concentration of the enzyme (in protomer units) to initiate the citrullination reaction. Samples were incubated at 37°C for 25 min in the same shaker. Reactions were quenched by flash freezing in liquid nitrogen. For color development, 2 mL of freshly prepared COLDER solution was added to the quenched reaction, vortexed to ensure complete mixing, and incubated for 15 min at 95°C. After cooling at room temperature, the samples were transferred into 1 mL-quartz cuvettes to be measured in the spectrophotometer. These control experiments were repeated twice.

Experiments with R29 and R97R105 were carried out similarly. Briefly, a solution containing 100 µM of each peptide was prepared in the "reaction buffer." The resulting solution was incubated for 15 min at 37°C in an Innova 4000 new Brunswick scientific incubator with a 150 rpm shaking. After such period, we added PADI4 to each of the solutions containing each peptide, to yield a final 0.7 µM concentration of the enzyme (in protomer units) to initiate the citrullination reaction. Samples were incubated at 37°C for 25 min in the same shaker. Reactions were quenched by flash freezing in liquid nitrogen. For color development, 2 mL of freshly prepared COLDER solution was added to the quenched reaction, vortexed to ensure complete mixing, and incubated for 15 min at 95°C. After cooling at room temperature, the samples were transferred into 1 mL-quartz cuvettes to be measured in the spectrophotometer. Also, these experiments were repeated twice.

As control experiments for the two peptides, in parallel, we prepared two solutions containing the same final concentration of each wild-type peptide, and the two samples were kept under the same experimental conditions as the other two peptide samples, but PADI4 was not added before the second incubation period.

1469896s, 2025, 2, Downloaded from https://onlinelibrary.wiley.com/doi/10.1002/pro.70033 by Universidad Miguel Hernández De Elche, Wiley Online Library on [29/10/2025]. See the Terms and Condition

# 4.8 | Isothermal titration calorimetry (ITC)

Calorimetric titrations for assessing the interaction of PADI4 with peptides from both series were carried out in an automated Auto-iTC200 high-sensitivity calorimeter (MicroCal, Malvern-Panalytical, Malvern, UK). Experiments were performed at 25°C in 20 mM Tris buffer (pH 7.5), 5 mM TCEP, 150 mM NaCl, and 5% glycerol. Peptide solution (200 µM) in the injection syringe was titrated into the PADI4 solution (20 μM in protomer units) in the calorimetric cell. A series of 19 injections with 2 μL volume, 0.5 μL/s injection speed, and 150 s time spacing was programmed while maintaining a reference power of 10 µcal/s and a stirring speed of 750 rpm. The heat effect per injection was calculated by integration of the raw data (thermal power as a function of time) after baseline correction. The interaction isotherm (ligand-normalized heat effect per injection as a function of the molar ratio) was analyzed through non-linear least-squares regression data analysis, applying a model that considers a single binding site to estimate the association constant,  $K_a$ , the interaction enthalpy,  $\Delta H$ , and the apparent stoichiometry of binding n (although, in practice, the last parameter usually reports the fraction of active protein in the sample within the calorimetric cell). The dissociation constant was calculated from the association constant:  $K_d = 1/K_a$ . The background injection heat (usually called "dilution heat," reflecting any unspecific phenomenon such as titrant/solute dilution, buffer neutralization, temperature equilibration, or solution mechanical mixing) was accounted for by including an adjustable constant parameter in the fitting routine. The data analysis was conducted in Origin 7.0 (OriginLab, Northampton, MA) with user-defined fitting functions.

# 4.9 | Biolayer interferometry (BLI)

# 4.9.1 | Experimental design of BLI experiments

The kinetic association  $(k_{\rm on})$  and dissociation  $(k_{\rm off})$  rate constants of the binding of both peptide series to PADI4 were determined by using a BLItz system (ForteBio Pall, Barcelona, Spain) (Frenzel & Willbold, 2014). The buffer used in the experiments was that recommended by the manufacturer. As PADI4 had a His-tag, it was immobilized on His-tag biosensors (Forte Bio) at the concentration of 0.45  $\mu$ M. The peptide concentration was varied in the range from 1 to 12  $\mu$ M during the association step.

The general schemes of the PADI4–peptide association/dissociation reactions in the BLItz system were: 30 s of acquisition of the initial baseline with the  $10\times$  kinetics buffer; 120 s of loading PADI4 into the biosensor; 30 s of baseline acquisition with the  $10\times$  kinetics buffer; 120 s of association of the peptide to the biosensor (which had been previously loaded with PADI4); and 120 s of dissociation of the peptide from the biosensor.

# 4.9.2 | Fitting of the sensorgrams

Fittings of the sensorgrams were carried out by using KaleidaGraph. The interferometry response during the association step (measured in response units, RU), R(t), and the binding rate, dR(t)/dt, were used to evaluate the kinetics of the formation of the PADI4/peptide complex, according to

$$\frac{dR(t)}{dt} = k_{\text{on}}[\text{peptide}](R_{\text{max}} - R(t)) - k_{\text{off}}R(t), \quad (2)$$

where  $R_{\rm max}$  is proportional to the total concentration of biosensor-bound PADI4; and [peptide] represents the corresponding concentration of a peptide from either the Ala21–Lys36 or Lys94–Val108 series.

In Equation (2), R(t) is given by

$$R(t) = R_{ea} - R_{ea} e^{(-k_{obs} (t - t_0))},$$
(3)

where  $R_{\rm eq}$  is the steady-state (or equilibrium) response obtained at an infinite time when  ${\rm d}R(t)/{\rm d}t=0$ , and  $t_0=180\,{\rm s}$  is the time at which the association step between biosensor-immobilized PADI4 and the peptide in the solution started. We fitted the experimentally obtained R(t) under any condition as

$$R(t) = R_{eq} - R_{eq} e^{(-k_{obs} (t - t_0))} - R'_{eq} (t - t_0). \tag{4}$$

The  $k_{\rm obs}$  was used for the pseudo-first-order plots, where its value is given by

$$k_{\text{obs}} = k_{\text{on}} [\text{peptide}] + k_{\text{off}}.$$
 (5)

The dissociation process was always fitted to a single exponential, with R(t) given by

$$R(t) = R_1 e^{(-k_{\text{off}}(t-t_0))},$$
 (6)

where  $t_0 = 300$  s is the time at which the dissociation of the peptide from the biosensor-bound PADI4 started in

our experimental set-up and  $R_1$  is the response level when dissociation starts.

Additional curves for the sections of the sensorgrams corresponding to the association step (Equation 5) for selected peptides are shown in Figure S7.

# 4.10 | Molecular modeling and simulation

Molecular docking simulations were performed to investigate the binding of the peptides to PADI4. The structure of the protein was built as previously described (Neira, Araujo-Abad, et al., 2022), on the basis of its crystallographic structure (Horikoshi et al., 2011) (entry 3APN in the Protein Data Bank), with missing atoms in a few loop regions reconstructed by using the Modeler server (Šali & Blundell, 1993) Peptides were built by using UCFS Chimera (Pettersen et al., 2004), and modified to add the correct cappings (acetylated and methylated at N and C termini, respectively). All protein/ peptide complexes were displayed by using PyMol 2.5.4 (https://www.pymol.org). In the first approach, molecular docking was performed by using the newly developed software DiffDock (Corso et al., 2022), which relies on a two-step diffusion-based generative approach: first a diffusion process generates a pose of the ligand by roto-translation and dihedral angle torsions, and then a confidence model is applied to estimate the binding score. Although still in development, DiffDock has attracted great attention because it outperforms other docking methods with a fast running time. A standard implementation was used, with default parameters: 20 inference steps (18 actual steps), 40 output samples, and no final step noise applied.

To investigate the binding of the wild-type peptides with a higher accuracy, the protein-peptide docking server MDockPeP was also used (Xu & Zou, 2020). This algorithm relies on the structure of the protein target and, due to the large variability of possible conformations in peptides, to their sole sequence as input. MDockPeP initially models non-redundant peptide conformers by using protein fragments with sequences similar to the template and then docks them independently on the protein surface by sampling binding modes with full flexibility (Yan et al., 2016). Docking runs were performed with default parameters, first on the whole structure of the PADI4 monomer and then on a selected region centered on the S atom of the catalytic residue Cys645 and with a size of the searching box of 50, 40, or 30 Å. The best docking poses were then re-scored by using the MM/GBSA technique (Rizzuti, 2022), as implemented in the HawkDock web server (Weng et al., 2019).

### SUPPLEMENTARY MATERIAL

There are four tables containing the <sup>1</sup>H assignments for the four peptides that were soluble. There are seven figures: the methyl region of the 1D-<sup>1</sup>H NMR spectra of the wild-type peptides of both series (Figure S1); the fluorescence titrations for Cit29 peptide of the Ala21–Lys36 series and the wild-type peptide of the Lys94–Val108 series (Figure S2); the ITC experiments for the Cit29 peptide in the absence of GSK484 (Figure S3); the far-UV CD spectra of the peptides of Lys94–Val108 series (Figure S4); the ITC experiments on the double mutant peptide (Figure S5); the six most favorable docking poses predicted for the wild-type peptides Ala21–Lys36 and Lys94–Val108 (Figure S6); and the association and dissociation curves of the sensorgrams from BLI experiments and their fittings for selected peptides (Figure S7).

#### **AUTHOR CONTRIBUTIONS**

José L. Neira: Conceptualization; formal analysis; writing - original draft; writing - review and editing; project administration; investigation; methodology; funding acquisition; validation. Bruno Rizzuti: Conceptualization; formal analysis; writing - original draft; writing - review and editing; software; methodology; investigation; validation. Martina Palomino-Schätzlein: Writing - review and editing; writing - original investigation. resources; Virginia Writing - original draft; writing - review and editing; resources; investigation. Olga Abian: Writing - original draft; writing - review and editing; funding acquisition; project administration. Adrian Velazquez-Campoy: Conceptualization; formal analysis; writing - original draft; writing - review and editing; funding acquisition; investigation; methodology; project administration.

### **FUNDING INFORMATION**

This research was funded by Spanish Ministry of Science and Innovation MCIN/AEI/10.13039/501100011033/ and "ERDF A way of Making Europe" [PID2021-127296OB-I00 to AVC]; by Instituto de Salud Carlos III co-funded by European Social Fund "Investing in your future" [PI18/00394 to OA]; by Diputación General de Aragón ["Protein targets and Bioactive Compounds group" E45 23R to AVC, and "Digestive Pathology Group" B25\_23R to OA]; by Consellería de Innovación, Universidades, Ciencia y Sociedad Digital (Generalitat Valenciana) [CIAICO 2021/0135 to AVC and JLN]; and by European Union "EXPLORA - Unlocking the Hidden Treasures of Aquatic Extremophiles: sustainable development of industrially relevant novel active biomolecules" [HORIZON-CL6-2024-CIRCBIO-01/101181841 to JLN]. The funders had no role in the study design, data

collection and analysis, decision to publish, or preparation of the manuscript.

The authors thank the three anonymous reviewers for helpful comments, suggestions, and discussions. They also thank Dr. Jeanine Amacher for handling the manuscript.

#### CONFLICT OF INTEREST STATEMENT

The authors have no relevant financial or non-financial interests to disclose.

### DATA AVAILABILITY STATEMENT

The datasets generated and/or analyzed during the current study are available from the corresponding authors upon reasonable request.

#### ORCID

José L. Neira https://orcid.org/0000-0002-4933-0428

Adrian Velazquez-Campoy https://orcid.org/0000-0001-5702-4538

#### REFERENCES

- Araujo-Abad S, Fuentes-Baile M, Rizzuti B, Bazán JF, Villamarin-Ortiz A, Saceda M, et al. The intrinsically disordered, epigenetic factor RYBP binds to the citrullinating enzyme PADI4 in cancer cells. Int J Biol Macromol. 2023;246:125632.
- Araujo-Abad S, Neira JL, Rizzuti B, García-Morales P, de Juan RC, Santofimia-Castaño P, et al. Intrinsically disordered chromatin protein NUPR1 binds to the enzyme PADI4. J Mol Biol. 2023; 435:168033. Available from. https://pubmed.ncbi.nlm.nih.gov/36858171/
- Araujo-Abad S, Rizzuti B, Soto-Conde L, Vidal M, Abian O, Velazquez-Campoy A, et al. Citrullinating enzyme PADI4 and transcriptional repressor RING1B bind in cancer cells. Int J Biol Macromol. Available from. 2024;274:133163. https://pubmed.ncbi.nlm.nih.gov/38878927/
- Araujo-Abad S, Rizzuti B, Villamarin-Ortiz A, Pantoja-Uceda D, Moreno-Gonzalez CM, Abian O, et al. New insights into cancer: MDM2 binds to the citrullinating enzyme PADI4. Protein Sci. 2023;32:e4723. Available from. https://pubmed.ncbi.nlm. nih.gov/37409874/
- Bax A. Davis DG (1985) MLEV-17-based two-dimensional homonuclear magnetization transfer spectroscopy. J Magn Reson. 1969; 65:355-60.
- Beckett D. Measurement and analysis of equilibrium binding titrations: a beginner's guide. Methods Enzymol. 2011;488:1–16.
- Birdsall B, King RW, Wheeler MR, Lewis CA, Goode SR, Dunlap RB, et al. Correction for light absorption in fluorescence studies of protein-ligand interactions. Anal Biochem. 1983;132:353–61.
- Cavanagh J, Fairbrother WJ, Palmer AGI, Skelton NJ. Protein NMR spectroscopy: principles and practice. San Diego: Elsevier Science; 1995.
- Cavanagh J. Rance M. Suppression of cross-relaxation effects in TOCSY spectra via a modified DIPSI-2 mixing sequence. J Magn Reson. 1992;96:670–8.

- Chakrabartty A, Kortemme T, Padmanabhan S, Baldwin RL. Aromatic side-chain contribution to far-ultraviolet circular dichroism of helical peptides and its effect on measurement of helix propensities. Biochem Int. 1993;32:5560–5. Available from. https://pubmed.ncbi.nlm.nih.gov/8504077/
- Chen F, Liu H, Sun H, Pan P, Li Y, Li D, et al. Assessing the performance of the MM/PBSA and MM/GBSA methods. 6. Capability to predict protein-protein binding free energies and re-rank binding poses generated by protein-protein docking. Phys Chem Chem Phys. 2016;18:22129–39. Available from. https://pubmed.ncbi.nlm.nih.gov/27444142/
- Chen J, Marechal V, Levine AJ. Mapping of the p53 and mdm-2 interaction domains. Mol Cell Biol. 1993;13:4107–14.
- Corso G, Stärk H, Jing B, Barzilay R, Jaakkola T. DiffDock: diffusion steps, twists, and turns for molecular docking. Available from 2022 https://arxiv.org/abs/2210.01776v2
- Danielsson J, Jarvet J, Damberg P, Gräslund A. Translational diffusion measured by PFG-NMR on full length and fragments of the Alzheimer A $\beta$ (1–40) peptide. Determination of hydrodynamic radii of random coil peptides of varying length. Magn Reson Chem. 2002;40:S89–97. Available from. https://doi.org/10.1002/mrc.1132
- Frenzel D, Willbold D. Kinetic titration series with biolayer interferometry. PLoS One. 2014;9:e106882.
- Gill SC, von Hippel PH. Calculation of protein extinction coefficients from amino acid sequence data. Anal Biochem. 1989; 182:319–26. Available from. https://pubmed.ncbi.nlm.nih.gov/2610349/
- Gudmann NS, Hansen NUB, Jensen ACB, Karsdal MA, Siebuhr AS. Biological relevance of citrullinations: diagnostic, prognostic and therapeutic options. Autoimmunity. 2015;48: 73–9. Available from. https://pubmed.ncbi.nlm.nih.gov/25520183/
- György B, Tóth E, Tarcsa E, Falus A, Buzás EI. Citrullination: a posttranslational modification in health and disease. Int J Biochem Cell Biol. 2006;38:1662–77. Available from. https://pubmed.ncbi.nlm.nih.gov/16730216/
- Horikoshi N, Tachiwana H, Saito K, Osakabe A, Sato M, Yamada M, et al. Structural and biochemical analyses of the human PAD4 variant encoded by a functional haplotype gene. Acta Crystallogr D Biol Crystallogr. 2011;67:112–8. Available from. https://pubmed.ncbi.nlm.nih.gov/21245532/
- Isert C, Atz K, Schneider G. Structure-based drug design with geometric deep learning. Curr Opin Struct Biol. Available from. 2023;79:102548. https://pubmed.ncbi.nlm.nih.gov/ 36842415/
- Ishigami A, Maruyama N. Importance of research on peptidylarginine deiminase and citrullinated proteins in age-related disease. Geriatr Gerontol Int. 2010;10:S53–8.
- Kearney PL, Bhatia M, Jones NG, Yuan L, Glascock MC, Catchings KL, et al. Kinetic characterization of protein arginine deiminase 4: a transcriptional corepressor implicated in the onset and progression of rheumatoid arthritis. Biochemistry. 2005;44:10570–82.
- Kelly SM, Jess TJ, Price NC. How to study proteins by circular dichroism. Biochim Biophys Acta. 2005;1751:119–39. Available from. https://pubmed.ncbi.nlm.nih.gov/16027053/
- Kjaergaard M, Brander S, Poulsen FM. Random coil chemical shift for intrinsically disordered proteins: effects of temperature and

- pH. J Biomol NMR. 2011;49:139–49. Available from. https://pubmed.ncbi.nlm.nih.gov/21234644/
- Kjaergaard M, Poulsen FM. Sequence correction of random coil chemical shifts: correlation between neighbor correction factors and changes in the Ramachandran distribution. J Biomol NMR. 2011;50:157–65. Available from. https://pubmed.ncbi.nlm.nih.gov/21604143/
- Knipp M, Vašák M. A colorimetric 96-well microtiter plate assay for the determination of enzymatically formed citrulline. Anal Biochem. 2000;286:257–64.
- Kumar A, Ernst RR, Wüthrich K. A two-dimensional nuclear Overhauser enhancement (2D NOE) experiment for the elucidation of complete proton-proton cross-relaxation networks in biological macromolecules. Biochem Biophys Res Commun. 1980;95:1–6. Available from. https://pubmed.ncbi.nlm.nih.gov/7417242/
- Kussie PH, Gorina S, Marechal V, Elenbaas B, Moreau J, Levine AJ, et al. Structure of the MDM2 oncoprotein bound to the p53 tumor suppressor transactivation domain. Science. 1996;274: 948–53. Available from. https://pubmed.ncbi.nlm.nih.gov/8875929/
- Lewis HD, Liddle J, Coote JE, Atkinson SJ, Barker MD, Bax BD, et al. Inhibition of PAD4 activity is sufficient to disrupt mouse and human NET formation. Nat Chem Biol. 2015;11:189–91. Available from. https://www.nature.com/articles/nchembio. 1735
- Li P, Wang D, Yao H, Doret P, Hao G, Shen Q, et al. Coordination of PAD4 and HDAC2 in the regulation of p53-target gene expression. Oncogene. 2010;29:3153–62.
- Li P, Yao H, Zhang Z, Li M, Luo Y, Thompson PR, et al. Regulation of p53 target gene expression by peptidylarginine deiminase 4. Mol Cell Biol. 2008;28:4758.
- Marion D, Wüthrich K. Application of phase sensitive twodimensional correlated spectroscopy (COSY) for measurements of (1)H-(1)H spin-spin coupling constants in proteins. 1983. Biochem Biophys Res Commun. 2012;425:519–26. Available from. https://pubmed.ncbi.nlm.nih.gov/22925668/
- McCoy MA, Gesell JJ, Senior MM, Wyss DF. Flexible lid to the p53-binding domain of human Mdm2: implications for p53 regulation. Proc Natl Acad Sci USA. 2003;100:1645–8. Available from. https://pubmed.ncbi.nlm.nih.gov/12552135/
- Momand J, Wu HH, Dasgupta G. MDM2--master regulator of the p53 tumor suppressor protein. Gene. 2000;242:15–29. Available from. https://pubmed.ncbi.nlm.nih.gov/10721693/
- Momand J, Zambetti GP, Olson DC, George D, Levine AJ. The mdm-2 oncogene product forms a complex with the p53 protein and inhibits p53-mediated transactivation. Cell. 1992;69: 1237–45.
- Mondal S, Thompson PR. Protein arginine deiminases (PADs): biochemistry and chemical biology of protein citrullination. Acc Chem Res. 2019;52:818–32. Available from. https://pubs.acs.org/doi/full/10.1021/acs.accounts.9b00024
- Neira JL, Araujo-Abad S, Cámara-Artigas A, Rizzuti B, Abian O, Giudici AM, et al. Biochemical and biophysical characterization of PADI4 supports its involvement in cancer. Arch Biochem Biophys. 2022;717:109125. Available from. https://linkinghub.elsevier.com/retrieve/pii/S0003986122000108
- Neira JL, Díaz-García C, Prieto M, Coutinho A. The C-terminal SAM domain of p73 binds to the N terminus of MDM2. Biochim Biophys Acta Gen Subj. 2019;1863:760–70.

- Neira JL, Hornos F, Bacarizo J, Cámara-Artigás A, Gómez J. The monomeric species of the regulatory domain of tyrosine hydroxylase has a low conformational stability. Biochemistry. 2016;55:3418–31.
- Neira JL, Rizzuti B, Abián O, Araujo-Abad S, Velázquez-Campoy A, de Juan RC. Human enzyme PADI4 binds to the nuclear carrier importin α3. Cells. 2022;11:2166. Available from. https://pubmed.ncbi.nlm.nih.gov/35883608/
- Neira JL, Rizzuti B, Abian O, Velazquez-Campoy A. Isolated autocitrullinated regions of PADI4 associate to the intact protein without altering their disordered conformation. Biophys Chem. 2024;312:107288. Available from. https://pubmed.ncbi.nlm.nih.gov/38991454/
- Pettersen EF, Goddard TD, Huang CC, Couch GS, Greenblatt DM, Meng EC, et al. UCSF chimera--a visualization system for exploratory research and analysis. J Comput Chem. 2004;25:1605–12. Available from. https://pubmed.ncbi.nlm.nih.gov/15264254/
- Piotto M, Saudek V, Sklenář V. Gradient-tailored excitation for single-quantum NMR spectroscopy of aqueous solutions. J Biomol NMR. 1992;2:661–5. Available from. https://pubmed. ncbi.nlm.nih.gov/1490109/
- Rizzuti B. Molecular simulations of proteins: from simplified physical interactions to complex biological phenomena. Biochim Biophys Acta, Proteins Proteomics. Available from. 2022;1870: 140757. https://pubmed.ncbi.nlm.nih.gov/35051666/
- Royer CA, Scarlata SF. Fluorescence approaches to quantifying biomolecular interactions. Methods Enzymol. 2008;450:79–106.
- Šali A, Blundell TL. Comparative protein modelling by satisfaction of spatial restraints. J Mol Biol. 1993;234:779–815. Available from. https://pubmed.ncbi.nlm.nih.gov/8254673/
- Serrano L, Matouschek A, Fersht AR. The folding of an enzyme. III. Structure of the transition state for unfolding of barnase analysed by a protein engineering procedure. J Mol Biol. 1992;224:805–18. Available from. https://pubmed.ncbi.nlm.nih.gov/1569558/
- Sharma P, Lioutas A, Fernandez-Fuentes N, Quilez J, Carbonell-Caballero J, Wright RHG, et al. Arginine citrullination at the C-terminal domain controls RNA polymerase II transcription. Mol Cell. 2019;73:84–96.e7. Available from. https://pubmed.ncbi.nlm.nih.gov/30472187/
- Uhrinova S, Uhrin D, Powers H, Watt K, Zheleva D, Fischer P, et al. Structure of free MDM2 N-terminal domain reveals conformational adjustments that accompany p53-binding. J Mol Biol. 2005;350:587–98.
- van Dieck J, Lum JK, Teufel DP, Fersht AR. S100 proteins interact with the N-terminal domain of MDM2. FEBS Lett. 2010;584: 3269–74. Available from. https://pubmed.ncbi.nlm.nih.gov/20591429/
- Vuilleumier S, Sancho J, Loewenthal R, Fersht AR. Circular dichroism studies of barnase and its mutants: characterization of the contribution of aromatic side chains. Biochem Int. 1993;32:10303–13. Available from. https://pubmed.ncbi.nlm.nih.gov/8399173/
- Wang Y, Chen R, Gan Y, Ying S. The roles of PAD2- and PAD4-mediated protein citrullination catalysis in cancers. Int J Cancer. 2021;148:267–76.
- Weeramange CJ, Fairlamb MS, Singh D, Fenton AW, Swint-Kruse L. The strengths and limitations of using biolayer interferometry to monitor equilibrium titrations of biomolecules. Protein Sci. 2020;29:1018–34. Available from. https://pubmed. ncbi.nlm.nih.gov/31943488/

- Weng G, Wang E, Wang Z, Liu H, Zhu F, Li D, et al. HawkDock: a web server to predict and analyze the protein-protein complex based on computational docking and MM/GBSA. Nucleic Acids Res. 2019;47:W322–30. Available from. https://pubmed.ncbi.nlm.nih.gov/31106357/
- Wilkins DK, Grimshaw SB, Receveur V, Dobson CM, Jones JA, Smith LJ. Hydrodynamic radii of native and denatured proteins measured by pulse field gradient NMR techniques. Biochem Int. 1999;38:16424–31. Available from. https://pubmed.ncbi.nlm.nih.gov/10600103/
- Witalison E, Thompson P, Hofseth L. Protein arginine deiminases and associated citrullination: physiological functions and diseases associated with dysregulation. Curr Drug Targets. 2015; 16:700–10.
- Xu X, Zou X. MDockPeP: a web server for blind prediction of protein-peptide complex structures. Methods Mol Biol. 2020; 2165:259–72. Available from. https://pubmed.ncbi.nlm.nih.gov/ 32621230/
- Yan C, Xu X, Zou X. Fully blind docking at the atomic level for protein-peptide complex structure prediction. Structure. 2016; 24:1842–53. Available from. https://pubmed.ncbi.nlm.nih.gov/ 27642160/
- Yang C, Dong ZZ, Zhang J, Teng D, Luo X, Li D, et al. Peptidylarginine deiminases 4 as a promising target in drug discovery. Eur J Med Chem. 2021;226:113840.

- Ying S, Dong S, Kawada A, Kojima T, Chavanas S, Méchin MC, et al. Transcriptional regulation of peptidylarginine deiminase expression in human keratinocytes. J Dermatol Sci. 2009;53: 2–9.
- Yuzhalin AE. Citrullination in cancer. Cancer Res. 2019;79:1274–84. Available from. https://aacrjournals.org/cancerres/article/79/7/1274/640899/Citrullination-in-CancerCitrullination-in-Cancer

#### SUPPORTING INFORMATION

Additional supporting information can be found online in the Supporting Information section at the end of this article.

How to cite this article: Neira JL, Rizzuti B, Palomino-Schätzlein M, Rejas V, Abian O, Velazquez-Campoy A. Citrullination at the N-terminal region of MDM2 by the PADI4 enzyme. Protein Science. 2025;34(2):e70033. <a href="https://doi.org/10.1002/pro.70033">https://doi.org/10.1002/pro.70033</a>